

Binary Classification as a Phase Separation Process

Rafael Monteiro

MONTEIRODASILVA-RAFAEL@AIST.GO.JP,
RAFAEL.A.MONTEIRO.MATH@GMAIL.COM

Mathematics for Advanced Materials Open Innovation Laboratory,
AIST, c/o Advanced Institute for Materials Research,
Tohoku University, Sendai, Japan

Abstract

We propose a new binary classification model called Phase Separation Binary Classifier (PSBC). It consists of a discretization of a nonlinear reaction-diffusion equation coupled with an Ordinary Differential Equation, and is inspired by fluids behavior, namely, on how binary fluids phase separate. Thus, parameters and hyperparameters have physical meaning, whose effects are studied in several different scenarios.

PSBC's equations can be seen as a dynamical system whose coefficients are trainable weights, with a similar architecture to that of a Recurrent Neural Network. As such, forward propagation amounts to an initial value problem. Boundary conditions are also present, bearing similarity with figure padding techniques in Computer Vision. Model compression is exploited in several ways, with weight sharing taking place both across and within layers.

The model is tested on pairs of digits of the classical MNIST database. An associated multiclass classifier is also constructed using a combination of Ensemble Learning and one versus one techniques. It is also shown how the PSBC can be combined with other methods - like aggregation and PCA - in order to construct better binary classifiers. The role of boundary conditions and viscosity is thoroughly studied in the case of digits "0" and "1".

Keywords: Binary classification, statistical machine learning, reaction-diffusion systems, finite-difference methods, Recurrent Neural Networks.

1. Introduction

In practical terms, classification is a task that humans and machines perform in many different situations: deciding whether an article is worth reading or not, labeling an image, classifying a device as defective or functional, or, in an abstract fashion, assigning an object X to one of the M classes $\{0, \dots, M-1\}$. When $M=2$ this process is called *binary classification*, which will be the main focus of this paper.

Several questions concerning classification are investigated in the field of Machine Learning (ML). Here we are interested in the particular case of binary classification using empirical risk minimization. We refer to "Devroye et al. (1996)" for a more theoretical approach to supervised learning, pointing out additional references along the way.

In binary classification one assumes the existence of an unknown map $h : \mathcal{X} \rightarrow \{0, 1\}$, conveniently called *hypothesis*, that one aims to investigate and somehow reconstruct, or approximate, from information available only on a subset of \mathcal{X} . In other words, given a data set (a sample) $\mathcal{D} := \{(X_{(i)}, Y_{(i)})\}_{1 \leq i \leq N_d} \subset \mathcal{X} \times \{0, 1\}$ and constraints

$$h(X_{(i)}) = Y_{(i)}, \quad (1.1)$$

one wishes to construct a map $\tilde{h} : \mathcal{X} \rightarrow \{0, 1\}$ that is a good approximation to $h(\cdot)$ in a certain sense. It's quality can be measured for instance

$$\text{Accuracy} = \frac{\text{cardinality} \left(\{i \in \{1, \dots, N_d\} \mid Y_{(i)} = \tilde{h}(X_{(i)})\} \right)}{N_d}, \quad (1.2)$$

which must then be maximized.¹

Since the constraints (1.1) are available for all $X_{(i)}$, this problem falls in the class of *supervised learning*. Writing $h(\cdot) = \mathbb{1}_{\mathcal{A}}(\cdot)$, where $\mathbb{1}_{\mathcal{A}}(x) = 1$ whenever $x \in \mathcal{A}$, 0 otherwise. Hence, constructing an approximation to $h(\cdot)$ is equivalent to finding - or rather “learning” - the unknown set $\mathcal{A} = h^{-1}(\{1\})$. Once an approximation $\tilde{h} : \mathcal{X} \rightarrow \{0, 1\}$ is constructed, it can be applied to any element in \mathcal{X} in order to “predict” whether it does, or does not, belong to \mathcal{A} ; consequently, one refers to $\tilde{h}(\cdot)$ as a *predictor*. Whenever a probability measure $\mu(\cdot)$ is considered in the space $\mathcal{X} \times \{0, 1\}$, discovering \mathcal{A} is called PAC learning; (Devroye et al., 1996, Chapter 12).

In the form just described the problem is too complex, for the space of functions $\{g(\cdot) \mid g : \mathcal{X} \rightarrow \{0, 1\}\}$ is too big and lacks mathematical structure. In practice, one follows the heuristics of choosing a smaller space of functions $\mathcal{H} \subset \{g(\cdot) \mid g : \mathcal{X} \rightarrow \{0, 1\}\}$ where $\tilde{h}(\cdot)$ is sought for. We call \mathcal{H} a *hypothesis space* (Cucker and Smale, 2002, §3).

We briefly describe one of the techniques developed to construct the map $\tilde{h}(\cdot)$, using *feedforward networks* (Goodfellow et al., 2016, Chapter 6): these are graph structures devoid of cyclic loops, as seen in the diagram in Figure 1.

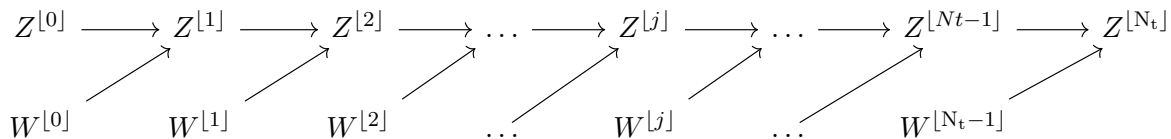


Figure 1: Unfolded graph of a forward propagation in a network with N_t layers and trainable weights $W^{[l]}$. An arrow from A to B indicates that B is a function of A .

For each $n \in \{0, \dots, N_t\}$ there exists an associated pair $(Z^{[n]}, W^{[n]}) \in \mathbb{R}^{z_n} \times \mathbb{R}^{w_n}$ referred to as a layer. When $n = 0$ and $n = N_t$, $Z^{[0]}$ and $Z^{[N_t]}$ are called respectively input layer (that receives input data from \mathcal{X}) and output layer; when $1 \leq n \leq N_t - 1$, the vectors $Z^{[n]}$ are called *hidden layers*. The variables $W^{[0]}, \dots, W^{[N_t-1]}$ are referred to as *trainable weights*, and are used for optimization purposes. Layers are all connected to each other in a hierarchical (that is, in a tree-like) fashion as

$$Z^{[n+1]} = \sigma^{[n]}(Z^{[n]}, W^{[n]}), \quad \text{for } 0 \leq n \leq N_t - 1. \quad (1.3)$$

The maps $\sigma^{[n]} : \mathbb{R}^{z_n} \times \mathbb{R}^{w_n} \rightarrow \mathbb{R}^{z_{n+1}}$ are called *activation functions* and can be endowed with different properties as differentiability, decay in the far-field, etc (Hastie et al., 2001). Last, one associates to this network a loss function $\mathcal{L}(Z, W, Y)$ that evaluates the sequence $Z = (Z^{[0]}, \dots, Z^{[N_t]})$ and its proximity to a given label $Y \in \{0, 1\}$ at a specific parameter value $W = (W^{[0]}, \dots, W^{[N_t-1]})$. Using the whole data set \mathcal{D} , these quantities make up a cost function $\text{Cost}_{\mathcal{D}}(\cdot)$ of the form

$$\text{Cost}_{\mathcal{D}}(W) = \sum_{i=1}^{N_d} \frac{\mathcal{L}(Z_{(i)}, W, Y_{(i)})}{N_d},$$

that one minimizes by optimization on W , as we explain next in detail.

Construction of $\tilde{h}(\cdot)$ from data is called *training* or *model fitting*, and is carried out using the network (1.3). First, one generates an initial sequence of trainable weights $W_0 := (W^{[0]}, \dots, W^{[N_t-1]})_0$ either randomly or deterministically. Then, for each pair of elements in $\mathcal{D} = \{(X_{(i)}, Y_{(i)})_{1 \leq i \leq N_d}\} \in$

1. Or minimizing the quantity $1 - \text{Accuracy} = \frac{\text{cardinality}(\{i \in \{1, \dots, N_d\} \mid Y_{(i)} \neq \tilde{h}(X_{(i)})\})}{N_d}$, called *misclassification error* (Devroye et al., 1996).

$\mathcal{X} \times \{0, 1\} = \mathbb{R}^{k_0} \times \{0, 1\}$ one sets $Z^{[0]} = X_{(i)}$ and generates a sequence $Z_{(i)} := (Z^{[0]}, \dots, Z^{[N_t]})_{(i)}$ using the feedforward network (1.3). Afterwards, W is updated using Gradient Descent,

$$W_{q+1} := W_q - \eta_q \frac{\partial \text{Cost}_{\mathcal{D}}(W)}{\partial W} \Big|_{W=W_q}, \quad q \in \mathbb{N}, \quad (1.4)$$

where W_q denotes the q -th iteration of this process.

Each iteration (1.4) to update W is called an *epoch*. The quantities η_q are positive numbers that receive the name of *learning rates* and may vary across epochs. The computation of sequences $Z_{(i)}$ is called *forward propagation*, while computing the derivatives of the cost with respect to Z and W is referred to as *backpropagation*. Altogether, the algorithmic organization of this process receives the name of *Backpropagation Algorithm* (BP), and is one of the cornerstones in the field of ML (Goodfellow et al., 2016, Chapter 6.5); see Figure 2.

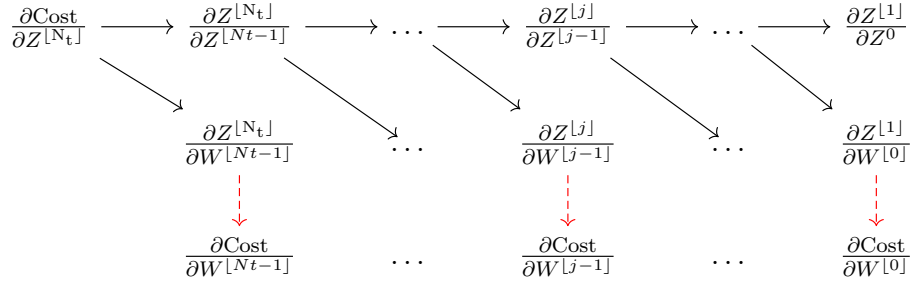


Figure 2: Classical Backpropagation algorithm. Its development was a major improvement in the design of the algorithms to perform gradient descent. Full arrows for A to B denote composition ($A \circ B$). Dashed arrows from A to B denote variable assignment ($A \leftarrow B$); see further details in the Supplementary Material.

Once iterations satisfy a stopping criteria (like tolerance, or some threshold), a parameter W_* is obtained, and a class assignment, or *discrimination rule*, takes place, corresponding in our case to

$$\tilde{h}(X_{(i)}) := \begin{cases} 1, & \text{if } \mathcal{L}(Z_{(i)}, W_*, 1) \leq \mathcal{L}(Z_{(i)}, W_*, 0), \\ 0, & \text{otherwise,} \end{cases} \quad (1.5)$$

finally completing the construction of $\tilde{h}(\cdot)$. There are several challenges presented along the way though: the structure of the cost function’s landscape can be very complex and in many applications optimizing with respect to W consists of a non-convex optimization problem, a difficulty that has received extensive attention from researchers in recent years.

Feedforward network architectures are ubiquitous in ML, appearing in Artificial Neural Networks (ANNs), Convolutional Neural Networks (CNNs), among other models, some of which are considered analogies to the brain or human vision functioning. To what extent these models just mimic or are a faithful description of any biological processes is unclear and sometimes disputed (Mumford, 1997); in this paper, however, we shall leave these considerations aside. We propose a new ML model whose motivation stems from a physical phenomenon by no means related to Biology nor (at least in principle) “brain-like” structures, but fluids and their dynamics: our model is inspired by how binary fluids phase separate.

In full generality, the model propagates features using two variables that evolve simultaneously,

$$\frac{U_m^{[n+1]} - U_m^{[n]}}{\Delta_t^u} := \frac{\varepsilon^2}{\Delta_x^2} \left(U_{m+1}^{[n+1]} - 2U_m^{[n+1]} + U_{m-1}^{[n+1]} \right) + f(U_m^{[n]}; \alpha_m^{[n]}), \quad \text{for } 1 \leq m \leq N_u, \quad (1.6a)$$

$$\frac{P_j^{[n+1]} - P_j^{[n]}}{\Delta_t^p} := f(P_j^{[n]}; \beta_j^{[n]}), \quad \text{for } 1 \leq j \leq N_p, \quad (1.6b)$$

where the nonlinearity $f(u, w) = u(1 - u)(u - w)$ is of the same type in both systems. Parameters $\alpha^{[l]}$ in $\beta^{[l]}$ are “trainable weights”, hence learned from data. We separate diffusion from non-linear effects by always taking $\Delta_x^2 := \Delta_t^u$. Initial conditions $U^{[0]}$ are individuals’ features, thus forward propagation amounts to an initial value problem, whereas $P^{[0]}$ is a fixed vector. Note that diffusion takes place in feature space.

Definition 1 (Phase Separation Binary Classifier - PSBC) *When a discrimination rule as in (1.5) is allied the numerical scheme (1.6), we say that we have a Phase Separation Binary Classifier, denoted in short as PSBC. As we discuss below, (1.6) falls in the class of feedforward networks, and in the sequel is also called PSBC model, whereas evolution of an initial condition is called forward propagation (see Figure 1). Whenever $\varepsilon = 0$ (resp., $\varepsilon > 0$) we refer to this classifier as non-diffusive PSBC (resp., diffusive PSBC).*

It is shown in Section 2.4 that the feedforward networks’ formulation (1.3) is sufficiently broad to encompass the PSBC model (1.6), then written as

$$\begin{pmatrix} U^{[n+1]} \\ P^{[n+1]} \end{pmatrix} := \sigma^{[n]} \left(U^{[n]}, W_u^{[n]}, P^{[n]}, W_p^{[n]} \right), \quad \text{with} \quad W_u^{[n]} := \alpha^{[n]}, \quad W_p^{[n]} := \beta^{[n]}.$$

Nevertheless, when compared with other state-of-art binary classifiers there are striking differences, many of which we investigate and highlight throughout the text. For instance: the first term on the right hand side of (1.6a), a discretization of the Laplacian, consists of a diffusion operator acting on features; $f(\cdot, \cdot)$ is a nonlinear reaction term that is common in thresholding phenomena, and mostly plays a role on classification of an individual $X_{(i)}$ into one of the elements in $\{0, 1\}$.

A quick description of each variable, without trying to fully elucidate their role at this point, goes as follows. The scalars $\Delta_t^u, \Delta_t^p > 0$ and $\varepsilon \geq 0$ are *hyperparameters* - quantities that are neither optimized, nor inputs in \mathcal{X} - and must be chosen in advance: the first two are due to time discretization, whereas the latter is a diffusion (or viscosity) term. We set $U^{[0]} = X \in \mathcal{X}$, with X representing features of an individual; thus, for each feature X_m we set $U_m^{[0]} := X_m$, $1 \leq m \leq N_u$. Note that $U^{[n]} \in \mathbb{R}^{N_u}$ for all layers, where N_u is the Euclidean dimension of \mathcal{X} . Boundary conditions of either Neumann or Periodic type affect the values of $U_0^{[l]}$ and $U_{N_u+1}^{[l]}$. A companion quantity $P^{[l]}$ evolves according to the ODE (1.6b) with initial condition $P_j^{[0]} = \frac{1}{2}$ for $1 \leq j \leq N_p$; its role that is clarified in Section 2.3. The vectors $\alpha^{[l]} \in \mathbb{R}^{N_u}$ and $\beta^{[l]} \in \mathbb{R}^{N_p}$ contain variables that must be optimized according to a cost function. The number N_p is either 1 or a value N_{pt} that indicates the dimension of the subspace where $\alpha^{[l]} \in \mathbb{R}^{N_u}$ lies; see discussion in Section 2.

Throughout this paper we write $U^{[l]}(X; \alpha^{[l]})$ to represent the flow of X through (1.6a) or, in a different terminology, we say that X is propagated by $U^{[l]}$; the same holds in the case $P^{[l]}(\frac{1}{2}; \beta^{[l]})$ with respect to (1.6b). In addition to that, we require a normalization condition of the initial data $X \in \mathcal{X}$,

$$X \in [0, 1]^{N_u}, \tag{1.7}$$

easily obtained by data preprocessing. As we shall see in Section 2.1, the main reason to enforce (1.7) is assuring that at any given epoch the forward propagation takes place inside an invariant region.

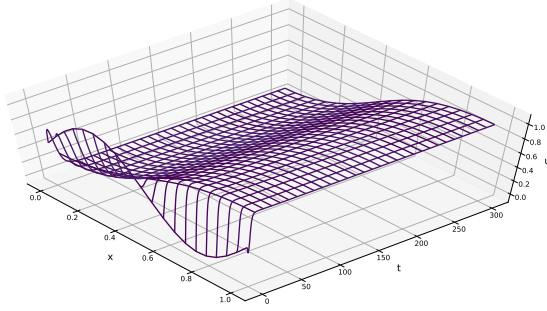
In order to explain other qualities of the PSBC we need to understand the numerical scheme (1.6) and its contrasting differences to other ML models. In the next section we present a succinct discussion of nonlinear diffusion equations, on which the mathematical and physical core of the PSBC model stand.

1.1 Mathematical setting: nonlinear diffusion equations

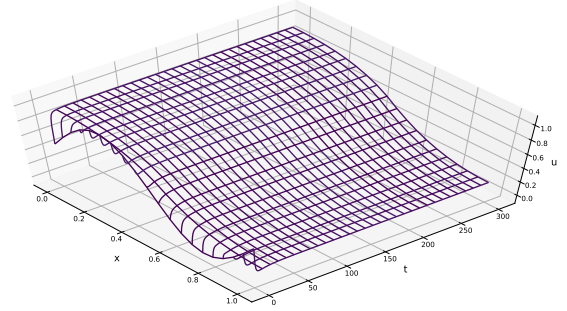
Clearly, the numerical scheme (1.6a) is a semi-implicit finite-differences discretization of

$$\begin{aligned} \partial_t u(x, t) &= \varepsilon^2 \partial_x^2 u(x, t) + u(x, t)(1 - u(x, t))(u(x, t) - \alpha(x)), \quad x \in [0, 1], \\ \partial_x u(0, t) &= 0, \quad \partial_x u(1, t) = 0, \quad u(x, 0) = u_0(x), \end{aligned} \quad (1.8)$$

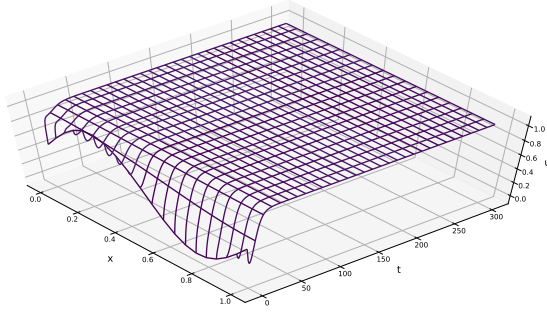
a nonlinear diffusion equation that describes phase separation in binary alloys and is known as *Allen-Cahn equation*. Equation (1.8) is one of the fundamental models in the theory of pattern formation (Dennis et al., 2015, IV.27).



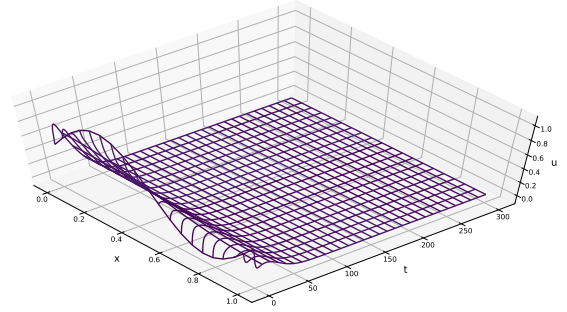
(a) $\alpha(x) = 4 - 8(x + 0.2)^2$.



(b) $\alpha(x) = -2 \cdot (\mathbb{1}_{(-\infty, 0.5)}(x) - \mathbb{1}_{[0.5, +\infty)}(x))$.



(c) $\alpha(x) = -0.8$.



(d) $\alpha(x) = 0.9$.

Figure 3: Numerical simulations of the Allen-Cahn Equation (1.8) using (1.6a) and different parameters $\alpha(\cdot)$. The initial conditions are fixed $u(x, t = 0) = \frac{1}{2} - \frac{1}{2} \sin(\pi(2x - 1))$, on $x \in [0, 1]$ with homogeneous Neumann boundary conditions. We use an uniform spatial grid with $N_u = 20$ points; $N_t = 300$, $\Delta_t^u = 0.1$, and $\varepsilon = 0.3$.

In Equation (1.8) time is represented by t , while x represents space. The scalar $u(x, t)$ denotes a macroscopic quantity that measures the relative proportion of two different species at (x, t) . The quantity $\varepsilon \geq 0$ represents a diffusive term, and for this reason we call the model diffusive (resp., non-diffusive) whenever $\varepsilon > 0$ (resp. $\varepsilon = 0$). Finally, $\alpha(\cdot) \in \mathbb{R}$ describes the medium's spatial heterogeneity, being paramount to understanding how the initial value problem associated to (1.8) evolves; some illustrative examples are shown in Figure 3.

Following ‘‘Angenent et al. (1987)’’, one can better understand the Allen-Cahn equation by first taking $\varepsilon = 0$ and $\alpha(\cdot) \in (0, 1)$: in this case, for each $x \in [0, 1]$ the dynamics in (1.8) decouples, yielding an ODE with two stable attracting points: $u \equiv 0$ and $u \equiv 1$. These limits are attained according to the initial state; namely, assuming that $\{x \in [0, 1] \mid u(x, 0) = \alpha(x)\}$ has measure zero, we have convergence (almost everywhere) to

$$\lim_{t \rightarrow \infty} u(x, t) = \begin{cases} 1, & \text{when } u(x, 0) > \alpha(x), \\ 0, & \text{when } u(x, 0) < \alpha(x). \end{cases} \quad (1.9)$$

Interestingly, the limiting function $\lim_{t \rightarrow \infty} u(x, t)$ assumes (almost everywhere) only two values, 0 and 1, in sharp contrast with $\alpha(\cdot)$ and the initial condition $u(\cdot, 0)$, both x -dependent. If we bear in mind the previous discussion, one can imagine an initial condition $u(\cdot, 0) := v^0(\cdot)$ as features of an individual with a class tag $Y \in \{0, 1\}$, where $\alpha(\cdot)$ is a parameter measuring correlations among features; as time evolves, the quantity $\alpha(\cdot)$ - in synergy with the nonlinearity $f(\cdot)$ - acts to classify $v^0(\cdot)$ in the “correct” way, which amounts to satisfying $\lim_{t \rightarrow \infty} u(\cdot, t; v^0) = Y$.

The mathematical study of (1.8) and other nonlinear diffusion equations is extensive. Under the framework of gradient-flows, it was shown in “Chafee (1975)” that, whenever $\alpha(\cdot)$ is a constant α , the only possible limit of (1.8) are constant solutions; consequently, in the case $0 < \alpha < 1$ this result implies that the only stable solutions are $u(\cdot) \equiv 0$ and $u(\cdot) \equiv 1$. Later on the interplay between geometry and dynamics was brought to the limelight in the seminal paper “Casten and Holland (1978)”, where it was proven that all stable solutions are constants also in the (spatial) multidimensional case, whenever the domain is convex (Ni, 2011, Chapter 2).

There is a drastic change in the behavior of (1.8) when $\alpha(\cdot)$ is allowed to be non-homogeneous in space. In such case a larger class of stable non-constant stationary solutions exist: it is shown in “Angenent et al. (1987)” that for some (non-constant) $\alpha(\cdot) \in C^1([-1, 1]; \mathbb{R})$ it is possible to construct stable stationary solutions $u(\cdot)$ that display several layers separating regions where $u(\cdot)$ is either close to 0 or close to 1 (Hale, 1988, Chapter 4, Sec. 4.3.8).

The previous discussion shows that different $\alpha(\cdot)$'s in (1.8) yield different asymptotic behaviors of solutions. Naturally, especially if we have binary classification in mind, the following question arises: given some fixed $T^* > 0$ (possibly $T^* = +\infty$), functions $v^0(\cdot)$ and $v^{T^*}(\cdot)$, is it possible to find a function $\alpha(\cdot)$ and an associated solution $u(x, t)$ to (1.8) such that

$$u(x, t) \Big|_{t=0} = v^0(x) \quad \text{and} \quad \lim_{t \uparrow T^*} u(x, t) = v^{T^*}(x)?$$

It is worth noticing that (1.8) is local but the equations to recover $\alpha(\cdot)$ are not, a common feature of inverse problems. With slightly more generality, we pose the previous question as a variational problem:

Problem 2 (Non-homogeneous α problem — continuum version) *Let \mathcal{B} and \mathcal{A} be Banach spaces, and assume that for any initial conditions in $v^0 \in \mathcal{X} \subset \mathcal{B}$ and $\alpha = \alpha(\cdot) \in \mathcal{A}$ the evolution model (1.8) exists and is represented by $u(x, t; v^0)$. Given a family $\left\{ \left(v_{(i)}^0(\cdot), v_{(i)}^{T^*}(\cdot) \right) \right\}_{i \in \Gamma} \in \mathcal{X} \times \mathcal{T} \subset \mathcal{B} \times \mathcal{B}$ (possibly uncountable), find the best $\alpha(\cdot) \in \mathcal{A}$, if attainable, that minimizes*

$$\lim_{t \uparrow T^*} \|u(\cdot, t; v_{(i)}^0) - v_{(i)}^{T^*}(\cdot)\|_{\mathcal{B}}. \quad (1.10)$$

Roughly speaking, the goal is that of reconstructing the heterogeneity of the media encoded $\alpha(\cdot)$. In other words, we aim to “learn $\alpha(\cdot)$ from data”, where data consists of pairs of initial conditions $u(\cdot, t) \Big|_{t=0} = v^0(\cdot) \in \mathcal{X}$ and target functions $v^{T^*}(\cdot) \in \mathcal{T}$.

A closely related but discrete formulation of Problem 2 is the backbone of the PSBC model.

Problem 3 (Non-homogeneous α problem — discrete version) *Let $N_t \in \mathbb{N}$. For all $0 \leq n \leq N_t$, denote by $(U^{[n]}(X; \alpha^{[n]}), P^{[n]}(\frac{1}{2}\mathbf{1}_{N_p}; \beta^{[n]})) \in \mathbb{R}^{N_u} \times \mathbb{R}^{N_p}$ the solution to the discretized PDE (1.6), of which $\alpha^{[n]} \in \mathbb{R}^{N_u}$ and $\beta^{[n]} \in \mathbb{R}^{N_p}$ are parameters. Given a map $\mathcal{F} : \mathbb{R}^{N_u} \times \mathbb{R}^{N_p} \rightarrow \mathbb{R}^{N_u}$ and a data set $\mathcal{D} = \{(X_{(i)}, Y_{(i)})_{1 \leq i \leq N_d}\} \subset \mathcal{X} \times \{0, 1\} \subset \mathbb{R}^{N_u} \times \{0, 1\}$, for all $0 \leq n \leq N_t - 1$ find $(\alpha^{[n]}, \beta^{[n]}) \in \mathbb{R}^{N_u} \times \mathbb{R}^{N_p}$ minimizing*

$$\text{Cost}_{\mathcal{D}}(\alpha^{[n]}, \beta^{[n]}) = \sum_{i=1}^{N_d} \frac{1}{N_d} \left\| \mathcal{F} \left(U^{[N_t]}(X_{(i)}, \alpha^{[n]}), P^{[N_t]}(\frac{1}{2}\mathbf{1}_{N_p}, \beta^{[n]}) \right) - Y_{(i)} \mathbf{1} \right\|_{\ell^2(\mathbb{R}^{N_u})}^2, \quad (1.11)$$

with discriminant function

$$\tilde{h}(X_{(i)}) := \begin{cases} 1, & \text{if } \|\mathcal{F}(\tilde{u}, \tilde{p}) - \mathbf{1}\|_{\ell^2(\mathbb{R}^{N_u})} \leq \|\mathcal{F}(\tilde{u}, \tilde{p})\|_{\ell^2(\mathbb{R}^{N_u})}^2, \\ 0, & \text{otherwise,} \end{cases} \quad (1.12)$$

where $(\tilde{u}, \tilde{p}) = (U^{\lfloor N_t \rfloor}(X_{(i)}, \alpha^{\lfloor \cdot \rfloor}), P^{\lfloor N_t \rfloor}(\frac{1}{2}\mathbf{1}_{N_p}, \beta^{\lfloor \cdot \rfloor}))$.

Let's clarify the similarities and differences between both problems. To begin with, imagine a simpler scenario where $\mathcal{F}(u, p) = u$. In this case, (1.11) becomes a discrete counterpart to (1.10). In reality, it will be shown that a more general map $\mathcal{F}(\cdot, \cdot)$, non-trivial and relying on the companion Equation (1.6b), is better suited for the classification task we are studying.

We should also observe that, unlike Problem 2, the target space in Problem 3 consists of a much simpler - binary - set that only contains the vectors $\mathbf{0}$ and $\mathbf{1}$ (respectively, vectors with only 0's, or 1's).² Discretization adds a high degree of flexibility to the problem, allowing both $\alpha^{\lfloor \cdot \rfloor}$ and $\beta^{\lfloor \cdot \rfloor}$ to either vary or repeat over layers. In this way, finding suitable trainable weights that minimize (1.11) is related to problems in optimal control.

Remark 4 (Equivalent discriminant functions) *It is more convenient to replace (1.11) by*

$$\widetilde{\text{Cost}}_{\mathcal{D}}(\alpha^{\lfloor \cdot \rfloor}, \beta^{\lfloor \cdot \rfloor}) = \sum_{i=1}^{N_d} \frac{1}{N_d} |\text{Mean}(\mathcal{F}(\tilde{u}, \tilde{p})) - Y_{(i)}|^2, \quad (1.13)$$

and (1.12) by the discriminant function

$$\tilde{\tilde{h}}(X_{(i)}) := \begin{cases} 1, & \text{if } |\text{Mean}(\mathcal{F}(\tilde{u}, \tilde{p})) - \mathbf{1}| \leq |\text{Mean}(\mathcal{F}(\tilde{u}, \tilde{p}))|, \\ 0, & \text{otherwise.} \end{cases} \quad (1.14)$$

where $(\tilde{u}, \tilde{p}) = (U^{\lfloor N_t \rfloor}(X_{(i)}, \alpha^{\lfloor \cdot \rfloor}), P^{\lfloor N_t \rfloor}(\frac{1}{2}\mathbf{1}_{N_p}, \beta^{\lfloor \cdot \rfloor}))$ and $\text{Mean}(v)$ denotes the average over the vector v 's entries. There are two reasons for doing this. First, because $\tilde{h}(\cdot)$ and $\tilde{\tilde{h}}(\cdot)$ are in fact the same discriminant function, as a direct expansion and rearrangement of both sides in the inequality (1.12) shows. Second, because (1.13) is computationally much cheaper than (1.11). For these reasons we shall adopt (1.13) over (1.11) in the rest of this paper.

1.2 Outline of the paper

This paper has two main goals: to introduce the PSBC, and to elaborate some of its fundamental mathematical properties, mostly by analysis of the numerical scheme (1.6). Since there are many hyperparameters and architectures to be accounted for we begin by taking the whole classifier apart, gradually reassembling it piece by piece, elucidating each parameter's functionality along the way.

We begin in Section 2, explaining the reasoning behind the model. The PSBC exploits model compression through a wide range of weights sharing architectures (Goodfellow et al., 2016, Chapter 7.9).

Definition 5 (Weight sharing among layers) *We say that a feedforward network (1.3) with N_t layers has layers- K -shared property whenever*

$$W = \left(W^{[0]}, \dots, W^{[N_t-1]} \right), \quad \text{with } W^{[i+j]} := W^{[i]} \quad \text{for } i \in K\mathbb{Z}, \quad j \in \{0, \dots, K-1\}.$$

Although the number of shared layers can take any value in the range $\{1, \dots, N_t\}$, in this paper we concentrate in two extreme cases: layers-1-shared (no shared layers; see Figure 1), and layers- N_t -shared (trainable weights repeat those in the first layer; see Figure 4).

2. This target space is not a vector space, just a subset of $\ell^2(\mathbb{R}^{N_u})$ with induced topology.

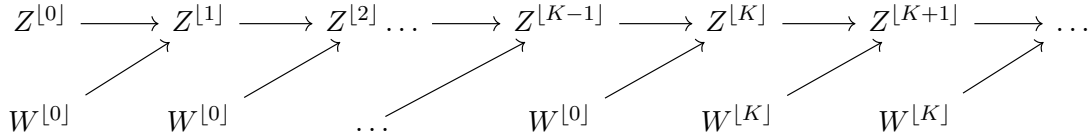


Figure 4: Unfolded graph of a forward propagation in a layers- K -shared architecture with N_t layers. An arrow from A to B indicates that B is a function of A . Whenever layer- N_t -shared architectures are considered, the model falls in the class of Recurrent Networks.

Other types of weight sharing will also be exploited, but take place within layers. For instance, further reduction on the number of trainable weights is attained by linear parameterization of $(\alpha^{[\cdot]})$ and $(\beta^{[\cdot]})$, as

$$\alpha^{[k]} = \mathcal{B}_u W_u^{[k]}, \quad \text{and} \quad \beta^{[k]} = \mathcal{B}_p W_p^{[k]}, \quad (1.15)$$

for $0 \leq k \leq N_t - 1$, where $\mathcal{B}_u \in \mathbb{R}^{N_u \times N_{pt}}$ and $\mathcal{B}_p \in \mathbb{R}^{N_u \times N_p}$.

Only a small set of parameters needs to be stored if both model’s architecture and suitable implementation are simultaneously taken advantage of; in this fashion, model compression enables efficient numerical parameterization. Weight sharing can also be seen as a regularization technique aiming to avoid over-fitting. Further motivation and technical details are given in Section 2

Still in Section 2, we turn our attention to numerical aspects of (1.6). Since (1.6a) is a semi-implicit (parabolic) scheme, there is an evident correspondence between forward propagation and the initial value problem associated with (1.6), therefore numerical stability issues have to be addressed.³ On one hand, the linear part of (1.6a) can be shown to be unconditionally stable for all values of Δ_t^u and Δ_x . On the other hand, when nonlinearities are included, blow-ups of $U^{[\cdot]}$ or $P^{[\cdot]}$ are possible, and must be analyzed with care.

Forward propagation also touches on the issue of global existence of the discrete dynamics (1.6). As trainable weights may vary from layer to layer, this question becomes even more challenging, paralleling that of a numerical scheme with variable coefficients. It is proven in Proposition 13 (and in earlier version of it, Proposition 8) that one can control the ℓ^∞ -norm of both $U^{[\cdot]}$ and $P^{[\cdot]}$ if constraints on Δ_t^u and Δ_t^p are imposed as

$$0 < \Delta_t^u \leq \frac{1}{\sqrt{3} \text{diameter}(\mathcal{R}_\alpha)^2}, \quad \text{and} \quad 0 < \Delta_t^p \leq \frac{1}{\sqrt{3} \text{diameter}(\mathcal{R}_\beta)^2}, \quad (1.16)$$

where both \mathcal{R}_α and \mathcal{R}_β are intervals constructed using $(\alpha^{[k]})_{0 \leq k \leq N_t - 1}$, and $(\beta^{[k]})_{0 \leq k \leq N_t - 1}$, respectively. For this reason we shall call the restrictions (1.16) on Δ_t^u and Δ_t^p *Invariant Region Enforcing Conditions*.

Section 3 is devoted to applications. We illustrate the PSBC’s properties by applying it to the classical MNIST database, a benchmark data set commonly used to assess the quality of several different ML models (Lecun et al., 1998). As a binary classifier, the model is evaluated on pairs of digits. Binary classifiers are used to construct a multiclass classifier in Section 3.2. A combination of Principal Components Analysis with the parameterization (1.15) is discussed, indicating possible directions of improvement. An extensive study of the roles of different boundary conditions, parameterization cardinality N_{pt} , and diffusion term ε is carried out for the sub data set of digits “0” and “1”.

3. Indeed, the numerical scheme (1.6a) can be seen as a particular case of

$$U^{[n+1]} = U^{[n]} + \theta \varepsilon^2 D_{N_u} U^{[n]} + (1 - \theta) \varepsilon^2 D_{N_u} U^{[n+1]} + \Delta_t^u f(U^{[n]}; \alpha^{[n]}). \quad \theta \in [0, 1],$$

If the nonlinearity is ignored, this model is known to be unconditionally stable when $0 \leq \theta \leq \frac{1}{2}$, that is, solutions remain stable for all values of Δ_t^u (Strikwerda, 1989, Section 6.3, page 147). A similar numerical scheme has also been exploited in “Hoff (1978)”.

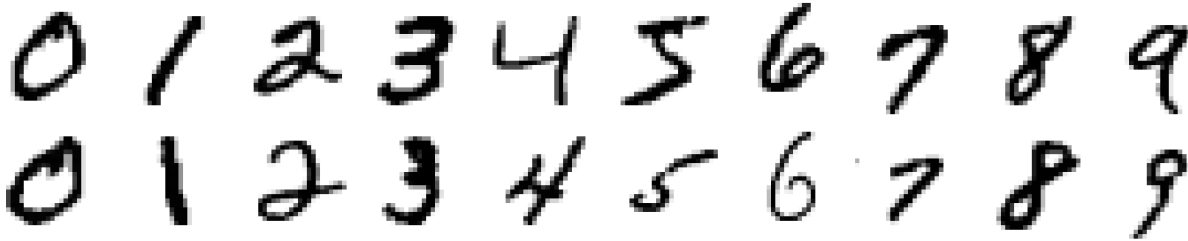


Figure 5: A sample from the MNIST database containing handwritten digits. Each picture has a shape 28×28 pixels, and is stored as a matrix; see the Appendix A for further information.

An extensive discussion in Section 4 closes the paper with several comments and open questions. Technical aspects of implementation and initialization of hyperparameters are described in the Appendix A. Lengthier mathematical results are fully derived in the Appendix B, devoted to discrete maximum principles, and in the Appendix C. Additional figures are left to the Supplementary Material.

1.3 Notation

Given a discrete Ordinary Differential Equation (ODE) or Partial Differential Equation (PDE), with initial condition $U^{[0]} = X \in \mathbb{R}^N$ we denote its n -th iteration step by $U^{[n]} = U^{[n]}(X) = \left(U_m^{[n]} \right)_{1 \leq m \leq N}$.

Vectors and column matrices are identified: we write both $a \in \mathbb{R}^n$, as well as $a \in \mathbb{R}^{n \times 1}$. Given the Euclidean space $E = \mathbb{R}^N$, whenever $V \in E$ we say that $V \geq 0$ if $V_m \geq 0$ for all $1 \leq m \leq N$. As such, $V \in \mathbb{R}_+^N$ means $V \geq 0$. Averaging is written as $\text{Mean}(V) = \frac{1}{N} \left(\sum_{m=1}^N V_m \right)$.

We write $\mathbb{G}_N := \{1, \dots, N\}$, calling $\text{supp}(V) = \{m \in \mathbb{G}_N | V_m \neq 0\}$ the support of V .

We denote by $\mathbf{1} \in E$ (resp. $\mathbf{0} \in E$) a vector with all the entries 1 (resp., 0); whenever disambiguation is necessary, we use $\mathbf{1}_N$ or $\mathbf{0}_N$ to indicate the dimension of the underlying space these vectors are in.

The canonical basis is defined as $e_i \in E$, $1 \leq i \leq N$. We shall further define

$$e_{\mathcal{A}} := \sum_{i \in \mathcal{A}} e_i, \quad \text{for } \mathcal{A} \subset \{1, \dots, N\} = \mathbb{G}_N. \quad (1.17)$$

Clearly, $e_{\{i\}} = e_i$, and $e_{\{1, \dots, N\}} = \sum_{i=1}^N e_i = \mathbf{1} = \mathbf{1}_N$. By abuse of notation, we shall use (1.17) for any Euclidean space, regardless of its dimension.

We shall say that a set \mathcal{A} is convex if for any $p, q \in \mathcal{A}$ we have that $\lambda p + (1 - \lambda)q \in \mathcal{A}$, for all $\lambda \in [0, 1]$. We write $\text{conv}(S)$ to denote the convex hull of a set S , which corresponds to the intersection of all convex sets containing S ; one can easily prove that the latter set is also convex.

Last, ANNs, CNNs, and RNNs are acronyms for Artificial Neural Networks, Convolutional Neural Networks, and Recurrent Neural Networks, respectively.

2. The reasoning behind the PSBC model

We begin our study of (1.6) by setting $\varepsilon = 0$, which yields an Euler discretization of an ODE,

$$U_m^{[n+1]} := U_m^{[n]} + \Delta_t^u f(U_m^{[n]}; \alpha_m^{[n]}), \quad \text{for } 1 \leq m \leq N_u, \quad U^{[0]} = X \in \mathbb{R}^{N_u}, \quad (2.1a)$$

$$P_j^{[n+1]} := P_j^{[n]} + \Delta_t^p f(P_j^{[n]}; \beta_j^{[n]}), \quad \text{for } 1 \leq j \leq N_p, \quad P^{[0]} = \frac{1}{2} \mathbf{1} \in \mathbb{R}^{N_p}. \quad (2.1b)$$

Since the nonlinearity $f(u, w) = u(1 - u)(u - w)$ is the same in both models all the existence results discussed next apply to both equations. For this reason we shall initially focus on (2.1a), postponing the discussion of the role of (2.1b) to Section 2.3.

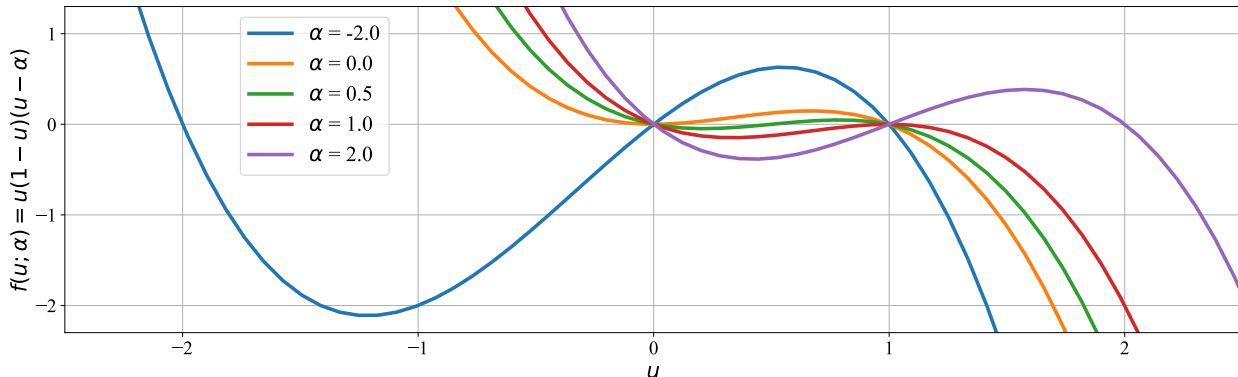
One of our main goals is verifying whether individual's features can be forward propagated through the network, namely, that $U^{[\cdot]}(X, \alpha^{[\cdot]})$ does not blow-up (causing a numerical overflow) before reaching the last layer of the network, where cost function evaluation and necessary optimization steps are taken. Notably and in contrast, models like ANNs, CNNs, and RNNs bypass this question by using squashing (bounded) activation functions (but not without trade-offs). In the PSCBC case, however, this concern is legitimate because Euler discretization methods do not have good stability properties (Iserles, 2009, Sec. 4.2). Fortunately, we show in Proposition 8 that control on the growth of $\|U^{[\cdot]}(X, \alpha^{[\cdot]})\|_{\ell^\infty}$ can be attained by adjustments on Δ_t^u (under the Normalized Condition 1.7).⁴ But first we explain why it is possible to control the growth of solution in (2.1), making a quick digression that takes us back to the Allen-Cahn Equation (1.8).

2.1 A glimpse on gradient flows and invariant regions on the continuum setting

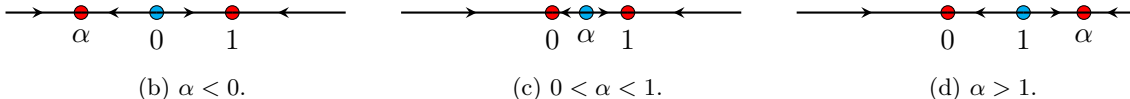
As said above, when $N_u = 1$ the numerical scheme (2.1) is a discretization of the ODE

$$\frac{du}{dt} = f(u; \alpha) := u(1 - u)(u - \alpha), \quad u(X, t = 0) = X \in \mathbb{R}, \quad \alpha \in \mathbb{R}. \quad (2.2)$$

The nonlinearity in (2.2) is of bistable type, with 3 stationary points: $u = 0$, $u = 1$, and $u = \alpha$. When α varies, the qualitative behavior of the stationary points 0 and 1 change, as we can see on the phase portrait of the ODE (2.2) in Figure 6.



(a) Sketches of the function $f(u; \alpha) = u(1 - u)(u - \alpha)$ for different values of α .



(b) $\alpha < 0$.

(c) $0 < \alpha < 1$.

(d) $\alpha > 1$.

Figure 6: Phase portraits of the ODE $\frac{d}{dt}u(t) = f(u; \alpha) = u(1 - u)(u - \alpha)$, for different values of α , with red (resp., blue) circles representing stable (resp., unstable) stationary points. Notice that in all the cases presented, the lowest and largest stationary points are stable, a fact that is exploited in the search for invariant regions, as explained in Section 2.3.

4. This is an example of nonlinear stabilization, since the region of A-stability of the Euler equations on the the region $\{z \in \mathbb{C} \mid \operatorname{Re}(z) \leq 0\}$ (Iserles, 2009, Chapter 4.2).

One can associate an energy functional $\mathcal{E}(u, \alpha) = - \int^u s(1-s)(s-\alpha)ds$ to (2.2), which now reads

$$\frac{du}{dt} = f(u; \alpha) := -\partial_u \mathcal{E}(u, \alpha), \quad \text{where } u(X, t=0) = X \in \mathbb{R}, \quad \alpha \in \mathbb{R}.$$

Consequently, along trajectories of (2.2) we must have

$$\frac{\partial}{\partial t} \mathcal{E}(u, \alpha) = -|\nabla_u \mathcal{E}(u, \alpha)|^2 \leq 0, \quad (2.3)$$

which can be interpreted as the rate of energy dissipated as the system evolves; these ideas and concepts can be generalized to systems and other functional spaces, and are an important tool in characterization of rate of convergence to asymptotic states (Carrillo et al., 2006, Sec. 2).

The phase portraits in Figure 6 indicate that the lowest and the largest stationary points of (2.2) are always either stable or semi-stable, regardless of the value α . In fact, using (2.3) and the structure of $\mathcal{E}(\cdot, \alpha)$, we can conclude that any interval \mathcal{I} containing the set

$$\Sigma_\alpha := [\min\{0, \alpha\}, \max\{1, \alpha\}] \quad (2.4)$$

is positively invariant with respect to (2.2), namely, whenever $x_0 \in \mathcal{I} \supset \Sigma_\alpha$ and \mathcal{I} is an interval, it holds that $u[x_0, t] \in \mathcal{I}$ for all $t \geq 0$ (Hirsch and Smale, 1974, Chapter 9). Similar ideas have been applied in PDEs, as discussed in Remark 20.

Naturally, this whole discussion readily extends to cases in which features lie in a high dimensional feature space. Indeed, with $\mathcal{E}(\cdot; \cdot)$ as given in Section 2.1 and $U \in \mathbb{R}^{N_u}$ for any $N_u \geq 1$, we can define a map $\tilde{\mathcal{E}} : \mathbb{R}^{N_u} \times \mathbb{R}^{N_u} \rightarrow \mathbb{R}$

$$\frac{dU}{dt} = -\nabla_U \tilde{\mathcal{E}}(U, \alpha), \quad \text{where } \tilde{\mathcal{E}}(U, \alpha) = \sum_{i=1}^{N_u} \mathcal{E}(U_i; \alpha_i), \quad (2.5)$$

which describes the dynamics (of features) as a gradient flow.

2.2 Back to the discrete setting: model compression and existence of dynamics ($\varepsilon = 0$)

Weight sharing within layers I. Although each entry of $\alpha^{[\cdot]}$ in (2.1a) can be optimized independently, a certain degree of flexibility - and model compression - can be achieved by parameterization of $\alpha^{[\cdot]}$; in this way we simultaneously generalize the model and reduce the number of trainable weights. This can be achieved by considering

$$\alpha^{[n]} = \mathcal{B}_u W_u^{[n]}, \quad \text{with } \mathcal{B}_u \in \mathbb{R}^{N_u \times N_{\text{pt}}} \quad \text{and} \quad W_u^{[n]} \in \mathbb{R}^{N_{\text{pt}}}. \quad (2.6)$$

In this paper we fix \mathcal{B}_u over layers, although this restriction can be removed. We refer to N_{pt} as *parameterization cardinality* and to \mathcal{B}_u as a *basis matrix*.

The specific form of \mathcal{B}_u is important and may be chosen according to the prediction problem; other possibilities are contemplated in Section 3.3. As we show next, under appropriate conditions on \mathcal{B}_u the ℓ^∞ norm of $\alpha^{[\cdot]}$ and $W_u^{[\cdot]}$ are proportional.

Lemma 6 *In order to avoid over-parameterization, assume that $N_{\text{pt}} \leq N_u$ and $\mathcal{B}_u = [b_1 | \dots | b_{N_{\text{pt}}}]$ has full rank (i.e., its columns are linearly independent). Then:*

- (i) (*Parameterization proportionality*) *It holds that $\|\alpha^{[n]}\|_{\ell^\infty} \approx \|W_u^{[n]}\|_{\ell^\infty}$, with constants depending on \mathcal{B}_u .*

(ii) (Decoupled evolution in terms of \mathcal{B}_u) The dynamics $U^{\lfloor \cdot \rfloor}(X)$ of any initial condition X through (2.1a) is so that each feature evolves independently. Furthermore, if $m \in \mathbb{G}_N$ is such that $m \notin \text{supp}(b_i)$, then the values in b_i do not affect the evolution of $U_m^{\lfloor \cdot \rfloor}(X)$.

The proof of (i) is immediate after rewriting (2.6) in its normal form $w = (\mathcal{B}_u^T \mathcal{B}_u)^{-1} \mathcal{B}_u \alpha$. Inspection of (2.1a) and (2.6) yields (ii). Lemma 6(i) shows that lower or upper bounds in terms of either $\alpha^{\lfloor \cdot \rfloor}$ or its parameters $W_u^{\lfloor \cdot \rfloor}$ are equivalent. Lemma 6(ii) on the other hand shows that the model has a parallelized architecture (see Remark 12).

Remark 7 (A canonical basis matrix construction) Let $1 \leq N_{\text{pt}} \leq N_u$, in such a way that $N_u = QN_{\text{pt}}$, for $Q \in \mathbb{N}$. Initially, set $\pi_0 := \emptyset$. For $1 \leq j \leq N_{\text{pt}}$, construct sets π_j recursively with the Q smallest elements in the set $\mathbb{G}_{N_u} \setminus \left(\bigcup_{l=0}^{j-1} \pi_l \right)$. Finally, define $\mathcal{B} := \left[e_{\pi_1} \mid \dots \mid e_{\pi_{N_{\text{pt}}}} \right]$ (recall notation in Section 1.3). For example, when $N_{\text{pt}} = N_u$ we get $\mathcal{B} = \text{Id}_{N_u}$, whereas when $N_{\text{pt}} = 1$ we obtain $\mathcal{B} = \mathbf{1}_{N_u}$. We stress that under this construction Lemma 6(i) holds as an equality, namely, $\|\alpha^{\lfloor \cdot \rfloor}\|_{\ell^\infty} = \|W_u^{\lfloor \cdot \rfloor}\|_{\ell^\infty}$. Other cases (like N_u and N_{pt} not multiple) are constructed similarly, and given in full generality in the Supplementary Material.

Forward propagation ($\varepsilon = 0$) — existence of dynamics We shall prove in this section, under mild conditions on Δ_t^u and the models' weights, that features can be forward propagated through the network and remain bounded. This is achieved by proving the existence of a bounded box where features start at - and remain inside - as the dynamics through (2.1a) unfolds.

The existence of such an invariant region immediately implies full control of lower and upper bounds of $u(t; \cdot)$ for all $t \geq 0$. Overall, it gives some type of stability of solutions up to possibly oscillatory behavior. Although the gradient flow structure is mostly lost upon discretization, it is shown in the next proposition that it can still be taken advantage of. Interestingly, numerical discretization yields an invariant set that is slightly bigger than the interval Σ_α in (2.4).

Proposition 8 (Global existence of forward propagation — inviscid case ($\varepsilon = 0$)) Let $N_t \in \mathbb{N}$ and $U^{\lfloor 0 \rfloor} := X \in [0, 1]^{N_u}$. Given two sequences of trainable weights $(\alpha^{\lfloor n \rfloor})_{0 \leq n \leq N_t - 1} \in \mathbb{R}^{N_u}$, augmented by $\alpha^{\lfloor -1 \rfloor} := \mathbf{1} \in \mathbb{R}^{N_u}$, denote by $U^{\lfloor \cdot \rfloor}(X, \alpha^{\lfloor \cdot \rfloor})$ the values obtained using (8). For any fixed $1 \leq v \leq N_u$ and $-1 \leq k \leq N_t - 1$, define the quantities

$$L_{\alpha, v}^{\lfloor k \rfloor} := \inf_{-1 \leq n \leq k} \left(\min \left\{ \alpha_v^{\lfloor n \rfloor}, 0 \right\} \right), \quad R_{\alpha, v}^{\lfloor k \rfloor} := \sup_{-1 \leq n \leq k} \left(\max \left\{ \alpha_v^{\lfloor n \rfloor}, 1 \right\} \right).$$

Assume that $-\infty < L_{\alpha, v}^{\lfloor N_t - 1 \rfloor}$ and $R_{\alpha, v}^{\lfloor N_t - 1 \rfloor} < +\infty$ hold, and that the Invariant Region Enforcing Condition (1.16) applies as

$$0 \leq \Delta_t^u \leq \min_{1 \leq v \leq N_u} \frac{1}{\sqrt{3} \left(|L_{\alpha, v}^{\lfloor N_t - 1 \rfloor}| + |R_{\alpha, v}^{\lfloor N_t - 1 \rfloor}| \right)^2}. \quad (2.7)$$

Then, for any $1 \leq v \leq N_u$ and $1 \leq q \leq N_p$ the sequences $U_v^{\lfloor k \rfloor}(X, \alpha^{\lfloor k \rfloor})$ and $P_q^{\lfloor k \rfloor}(X, \beta^{\lfloor k \rfloor})$ satisfy

$$L_{\alpha, v}^{\lfloor k-1 \rfloor} - \Delta_t^u M_{\alpha, v}^{\lfloor k-1 \rfloor} \leq U_v^{\lfloor k \rfloor}(X, \alpha^{\lfloor k \rfloor}) \leq R_{\alpha, v}^{\lfloor k-1 \rfloor} + \Delta_t^u M_{\alpha, v}^{\lfloor k-1 \rfloor}, \quad (2.8)$$

for all $0 \leq k \leq N_t$ and $M_{(\alpha, \cdot)}^{\lfloor k \rfloor} := \left(|L_{(\alpha, \cdot)}^{\lfloor k \rfloor}| + |R_{(\alpha, \cdot)}^{\lfloor k \rfloor}| \right)^3$.

In particular, $|U_v^{\lfloor k \rfloor}(X, \alpha^{\lfloor k \rfloor})| \leq (1 + \Delta_t^u) M_{\alpha, v}^{\lfloor k-1 \rfloor}$ holds for all $0 \leq k \leq N_t$.

The previous results will be mostly used in the following way.

Corollary 9 *Proposition 8 still holds with $L_{\alpha,v}^{[k]}$ and $R_{\alpha,v}^{[k]}$ substituted respectively by $L_{\alpha}^{[k]}$ and $R_{\alpha}^{[k]}$, where*

$$L_{\alpha}^{[k]} := \inf_{-1 \leq n \leq k} \left(\min_{1 \leq v \leq N_u} \{ \alpha_v^{[n]}, 0 \} \right) \quad R_{\alpha}^{[k]} := \sup_{-1 \leq n \leq k} \left(\max_{1 \leq v \leq N_u} \{ \alpha_v^{[n]}, 1 \} \right).$$

In this case, (2.8) reads as

$$(L_{\alpha}^{[k-1]} - \Delta_t^u M_{\alpha}^{[k-1]}) \mathbf{1} \leq U^{[k]}(X, \alpha^{[k]}) \leq (R_{\alpha}^{[k-1]} + \Delta_t^u M_{\alpha}^{[k-1]}) \mathbf{1},$$

with $M_{\alpha}^{[k]} := (|L_{\alpha}^{[k]}| + |R_{\alpha}^{[k]}|)^3$.

A proof of this result is found in the Appendix C. It is important to observe that these bounds do not depend on N_t , and may vary for different epochs: the result does not say how the invariant region evolves throughout the training process, and in fact it is not clear whether there exists such an invariant region for trainable weights. Nevertheless, training relies on Gradient Descent, thereby a synergy between the ℓ^∞ -norm growth of $U^{[\cdot]}(X, \alpha^{[\cdot]})$ and that of W_u is expected.

2.3 Bringing in the phase equation, coupling both models, and further model compression

We finally explain why (2.1) is made up of two systems of equations. It turns out that, unfortunately, just using (1.6a) for learning is doomed to failure, a fact that we explain with the help of the next result. (The proof is found in the appendix.)

Lemma 10 (Monotonicity yields “non-learnable” classes) *Let $X, \tilde{X} \in \mathbb{R}$ be two individuals satisfying the normalization condition (1.7). Fix $0 \leq \Delta_t^u < \frac{1}{10}$, and consider (2.1a) with $N_u = 1$. The discrimination rule (1.14) takes the form $h(X_{(i)}) = 1$, if $U^{[N_t]}(\tilde{X}; \alpha^{[N_t-1]}) \geq \frac{1}{2}$, and $h(X_{(i)}) = 0$ otherwise. Then, whenever $X \geq \tilde{X}$, we have $U^{[n]}(X; \alpha^{[n]}) \geq U^{[n]}(\tilde{X}; \alpha^{[n]})$, for all $0 \leq n \leq N_t$.*

The consequences of this result can be seen in an illustrative example. For a fixed $\gamma^* \in (0, 1)$, let's label the data as $Y_{(i)} = \mathbb{1}_{\{z \leq \gamma^*\}}(X_{(i)})$, and take (X, Y) and (\tilde{X}, \tilde{Y}) satisfying $X > \gamma^* \geq \tilde{X}$. Under these assumptions we claim that at least one of them is wrongfully classified. Indeed, assume that both individuals are correctly classified. Labeling and features' properties imply that $Y = 0$ and $\tilde{Y} = 1$, hence we must have $U^{[N_t]}(X; \alpha^{[N_t-1]}) < \frac{1}{2} \leq U^{[N_t]}(\tilde{X}; \alpha^{[N_t-1]})$. However, since $X > \tilde{X}$, this violates Lemma 10.

In a few words, a model that consists of (2.1a) only has a flaw: it strongly depends on label assignment.

Equation (2.1b) is introduced to repair this issue. The fixing is easily motivated by considering the 1D case in the continuum setting (2.2): first, we construct two linear maps,

$$\mathcal{S}_1^{(0)}(u) = u, \quad \mathcal{S}_1^{(1)}(u) = 1 - u, \quad u \in \mathbb{R}.$$

Observe that $\mathcal{S}_1^{(1)}(0) = 1$ and $\mathcal{S}_1^{(1)}(1) = 0$; in other words, $\mathcal{S}_1^{(1)}(\cdot)$ flips the interval $[0, 1]$, whereas $\mathcal{S}_1^{(0)}(\cdot)$ is simply the identity map. Such properties convey all that is needed: we choose $\mathcal{S}_1^{(0)}(\cdot)$ when no relabeling is needed, otherwise we choose $\mathcal{S}_1^{(1)}(\cdot)$ and flip the labels, applying the previous model to $\mathcal{S}_1^{(1)}(U^{[\cdot]}; \alpha^{[\cdot]})$. In practice, figuring out when to use either of these maps involves the construction of a homotopy,

$$\mathcal{S}_1^{(p)}(u) := (1 - p) \mathcal{S}_1^{(0)}(u) + p \mathcal{S}_1^{(1)}(u), \quad (2.9)$$

reducing matters to that of “learning” the homotopy parameter p .⁵ The type of nonlinearity found in (2.2) can be used for such purpose, namely, by setting $\frac{dp}{dt} = f(p; \beta) := p(1-p)(p-\beta)$, with $p(0) = \frac{1}{2}$. Now, $p = p(\cdot)$ has the desired properties as long as we learn the parameter β . In the end, going back to the continuum model, fixing the labels consists in obtaining $\lim_{t \rightarrow \infty} \mathcal{S}_1^{(p(t))}(u(X_{(i)}, t; \alpha)) = Y_{(i)}$, which is achieved depending on the asymptotic behavior of $p(t)$ as $t \rightarrow \infty$.

A multidimensional version of (2.9), more necessary to our goals, is given by

$$\mathbb{R}^{N_u} \times \mathbb{R}^{N_u} \ni (p, u) \mapsto \mathcal{S}_{N_u}^{(p)}(u) := (\mathbf{1} - p) \circledast \mathcal{S}_{N_u}^{(0)}(u) + p \circledast \mathcal{S}_{N_u}^{(1)}(u). \quad (2.10)$$

where both $\mathcal{S}_{N_u}^{(0)}(u) = u$ and $\mathcal{S}_{N_u}^{(1)}(u) = \mathbf{1} - u$ are maps from \mathbb{R}^{N_u} to itself.

After all this discussion, still, more model compression can be attained.

Weight sharing within layers II. Given elements $(X_{(i)}, Y_{(i)})$ in a data set, we would like to adjust parameters in Equation (1.6) in such a way that $\mathcal{S}_{N_u}^{(p)}(U^{[N_t]}(X_{(i)}; \alpha))$ “approximates” $Y_{(i)}\mathbf{1}$. Since the role of $p \in \mathbb{R}^{N_u}$ in (2.10) is that of fixing label dependency, it will be taken by Equation (1.6b). Hence, an immediate candidate consists of taking $p = P^{[N_t]}\mathbf{1}_{N_u} \in \mathbb{R}^{N_u}$, where $P^{[\cdot]}$ evolves according to (1.6b), with $N_p = 1$.

Among several other possible constructions of p , one that we adopt in this paper relies on weight sharing. We once again use linear parameterizations: first, let $U^{[\cdot]}$ be a solution to (2.1a) in such a way that the relation (2.6) holds. Recall from Lemma 6(ii) that $U_m^{[\cdot]}$ depends only on columns b of \mathcal{B}_u where $m \in \text{supp}(b)$. Thanks to this “evolutionary independence”, one can associate a unique 1D equation of the form (2.1b) to each of these columns, each with a similar role as that of p in (2.9). Altogether, that would require coupling (2.1a) with a system of equations of the form (2.1b), with $N_p = N_{\text{pt}}$ variables.

We use (2.10) to summarize these two cases.

Definition 11 (Subordinate and non-subordinate models) *Given $1 \leq N_{\text{pt}} \leq N_u$ and a basis matrix \mathcal{B}_{sub} as in (2.6). Then, two constructions are available:*

(i) **(Non-subordinate phase)** *Set $N_p := 1$ (hence, $P^{[\cdot]} \in \mathbb{R}$) and $\mathcal{B}_{\text{sub}} = \mathbf{1}_{N_u} \in \mathbb{R}^{N_u \times 1}$. Define*

$$\widetilde{P^{[N_t]}} := \mathcal{B}_{\text{sub}} \cdot P^{[N_t]} = P^{[N_t]}\mathbf{1}_{N_u} \in \mathbb{R}^{N_u},$$

where $P^{[\cdot]}$ evolves by (1.6b).

(ii) **(Subordinate phase)** *Set $N_p := N_{\text{pt}}$ (hence, $P^{[\cdot]} \in \mathbb{R}^{N_{\text{pt}}}$). Define*

$$\widetilde{P^{[N_t]}} := \mathcal{B}_{\text{sub}} \cdot P^{[N_t]} = \sum_{j=1}^{N_{\text{pt}}} P_j^{[N_t]} e_{\pi_j^*} \in \mathbb{R}^{N_u}, \quad \text{for } P^{[N_t]} = \begin{bmatrix} P_1^{[N_t]} \\ \vdots \\ P_{N_{\text{pt}}}^{[N_t]} \end{bmatrix} \in \mathbb{R}^{N_{\text{pt}}},$$

where $P^{[\cdot]}$ evolves by (1.6b).

Thus, for any chosen subordination, we couple (2.1a) with the system (2.1b) (with N_p variables). Last, we make use of (2.6) once more, parameterizing $\beta^{[\cdot]} = \mathcal{B}_p W_p^{[\cdot]}$; this time, $\mathcal{B}_p = \text{Id}_{N_p}$.

5. Throughout the numerics the value of p may scape the range $[0, 1]$, but in terms of modeling it does what is intended, for optimization in β is also in place. Similar maps are used in some gated RNN architectures; cf. (Goodfellow et al., 2016, Chapter 10.10).

Using this construction we are now ready to use the model (2.1) after combining it with a cost function,

$$\widetilde{\text{Cost}}_{\mathcal{D}} = \frac{1}{2N_d} \sum_{i=1}^{N_d} \left| \text{Mean} \left(\mathcal{S}_{N_u}^{(P^{[\cdot]})} \left(U^{[N_t]} (X_{(i)}; \alpha) \right) \right) - Y_{(i)} \right|_{\ell^2(\mathbb{R}^{N_u})}^2, \quad (2.11)$$

which is then optimized for $\alpha^{[\cdot]} = \mathcal{B}_u W_u^{[\cdot]}$ and $\beta^{[\cdot]} = \mathcal{B}_p W_p^{[\cdot]}$ (not shown, but implicit in the dynamics of (2.1b)). We highlight that the cost function introduces interaction between parameters $\alpha^{[\cdot]}$ and $\beta^{[\cdot]}$.

Different types of layers are illustrated in Figure 7.

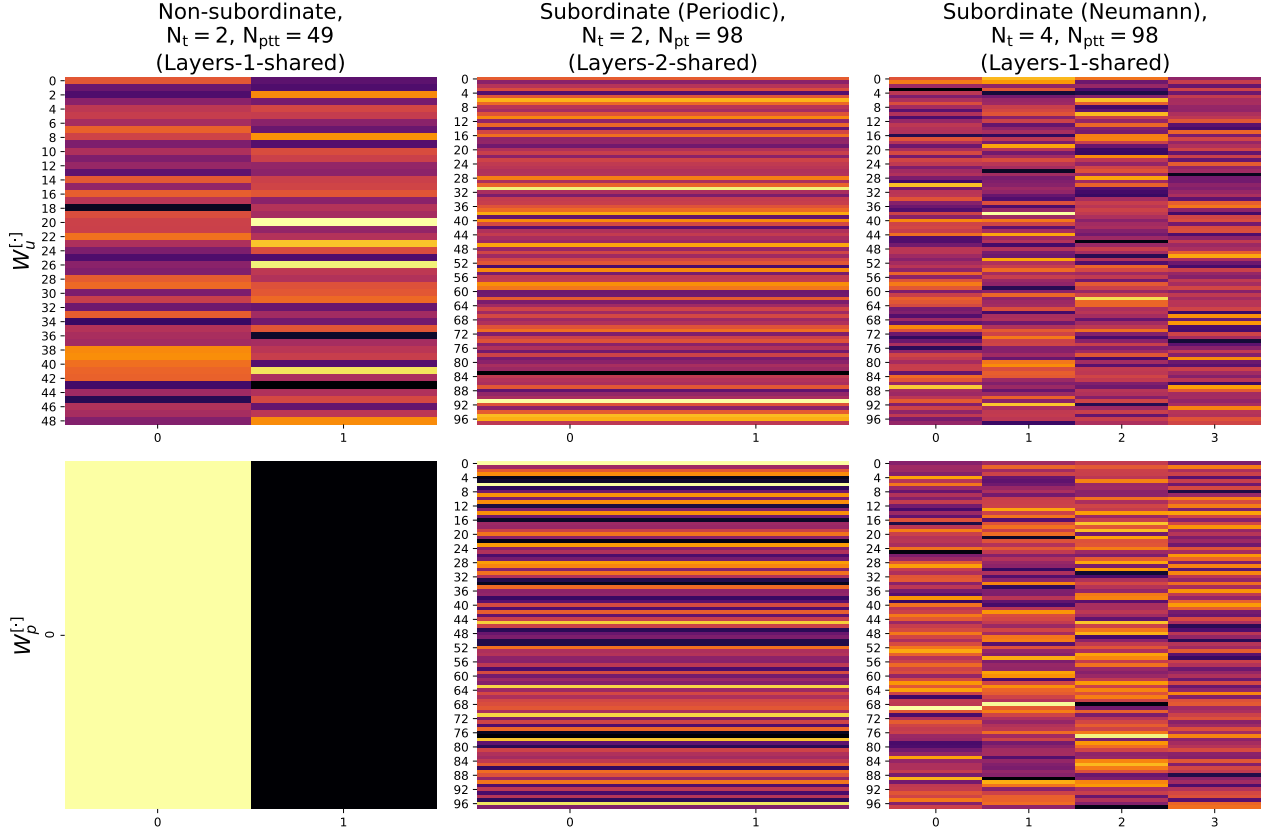


Figure 7: Heatmaps of trainable weights for the PSBC with different architectures.

Remark 12 (Model parallelization) *In real applications of ML, due to the growing size of data sets, nearly all models rely on some sort of data parallelization (processing data in parts) using techniques like (minibatch) Stochastic Gradient Descent. On the other hand, achieving model parallelization (in which the model itself is split in fully independent parts) is much more complicated and an intense topic of research, with important practical implications to Engineering and Computer Science.*

It turns out that model parallelization can be obtained whenever $\varepsilon = 0$ using canonical basis matrices for \mathcal{B}_u , \mathcal{B}_p , and \mathcal{B}_{sub} , as described above. In this way, due to Lemma 6(ii), features are forward propagated by $U^{[\cdot]}$ and $P^{[\cdot]}$ as N_{pt} decoupled problems. Moreover, optimization splits into N_{pt} smaller instances, that can be minimized independently.

2.4 Forward propagation ($\varepsilon \geq 0$) — existence of dynamics

In light of Lemma 6(ii), the use of basis matrices constructed as in Remark 7 imply that features do not “interact” during forward propagation, which can be problematic because correlations are not fully

captured until the cost function is evaluated. We can mitigate this by adding to (2.5) a penalization term of the form $\frac{\varepsilon}{2} \sum_{m=1}^{N_u} \left| U_m^{[l]} - U_{m+1}^{[l]} \right|^2$, with due adjustments to account for boundary conditions; the strength of this penalization is controlled by a diffusion parameter ε . Evidently, we do not add a similar term to $P^{[l]}$'s equation, whose main goal is to fix any possible label dependency.

At first we limit ourselves to homogeneous boundary conditions of Neumann type,

$$U_0^{[n]} := U_{+2}^{[n]}, \quad \text{and} \quad U_{N_u+1}^{[n]} := U_{N_u-1}^{[n]}, \quad \forall n \in \mathbb{N}.$$

The connection between the PSBC and the feedforward network description in Figure 1 becomes more pronounced if we rewrite (1.6a) in vectorial form,

$$\mathbf{L}_{N_u} U^{[n+1]} = U^{[n+1]} - \varepsilon^2 \mathbf{D}_{N_u} U^{[n+1]} = U^{[n]} + \Delta_t^u f(U^{[n]}; \alpha^{[n]}), \quad (2.12)$$

where

$$\mathbf{L}_{N_u} := \text{Id}_{N_u} - \varepsilon^2 \mathbf{D}_{N_u}, \quad \text{with} \quad \mathbf{D}_{N_u} = \begin{bmatrix} -2 & 2 & 0 & \dots & 0 \\ 1 & -2 & 1 & \dots & 0 \\ 0 & 1 & -2 & \dots & 0 \\ \vdots & \ddots & \ddots & -2 & 1 \\ 0 & & 0 & 2 & -2 \end{bmatrix} \in \mathbb{R}^{N_u \times N_u}. \quad (2.13)$$

A similar formula holds for (1.6b), with $\mathbf{L}_{N_p} := \text{Id}_{N_p}$. A direct application of Gershgorin's Theorem implies that \mathbf{L}_{N_u} is invertible for all $\Delta_t^u \geq 0$, $\varepsilon \geq 0$ (Dym, 2007, Theorem 20.12). Therefore, (2.12) reads as

$$U^{[n+1]} = \mathbf{L}_{N_u}^{-1} \cdot \left(U^{[n]} + \Delta_t^u f(U^{[n]}; \alpha^{[n]}) \right). \quad (2.14)$$

Now, writing $Z^{[n]} := \begin{pmatrix} U^{[n]}(X, \alpha^{[n]}) \\ P^{[n]}(\frac{1}{2}\mathbf{1}, \beta^{[n]}) \end{pmatrix}$, with $\alpha^{[n]} = \mathcal{B}_u \cdot W_u^{[n]}$ and $\beta^{[n]} = \mathcal{B}_p \cdot W_p^{[n]}$, we define the activation function $\sigma^{[n]}(\cdot, \cdot, \cdot, \cdot)$ as a map from $\mathbb{R}^{N_u} \times \mathbb{R}^{N_u} \times \mathbb{R}^{N_p} \times \mathbb{R}^{N_p}$ to itself,

$$\sigma^{[n]}(U, W_u, P, W_p) := \begin{pmatrix} (\mathbf{L}_{N_u})^{-1} \cdot (U + \Delta_t^u f(U, W_u)) \\ P + \Delta_t^p f(P, W_p) \end{pmatrix}. \quad (2.15)$$

Thus, we can write the discrete evolution (1.6) using the general framework presented in (1.3),

$$Z^{[n+1]} = \begin{pmatrix} U^{[n+1]} \\ P^{[n+1]} \end{pmatrix} = \sigma^{[n]} \left(U^{[n]}, W_u^{[n]}, P^{[n]}, W_p^{[n]} \right) = \sigma^{[n]} \left(Z^{[n]}, W^{[n]} \right). \quad (2.16)$$

It is also possible to study the PSBC model with periodic boundary conditions (when $N_u \geq 3$), taking $U_0^{[n]} := U_{N_u}^{[n]}$, and $U_{N_u+1}^{[n]} := U_1^{[n]}$, for all $n \in \mathbb{N}$. In such case a different diffusion matrix $\mathbf{D}_{N_u}^{(\text{per})}$ is obtained, but all the results related to the Invariant Region Enforcing Condition remain valid (mainly because Maximum Principles still hold; see Appendix B).

Proposition 8 and Corollary 9 can be generalized to contemplate the dynamics in (1.6).

Proposition 13 (Global existence of forward propagation — general case) *Let $N_t \in \mathbb{N}$ and $U^{[0]} := X \in [0, 1]^{N_u}$. Given trainable weights $(\alpha^{[n]})_{0 \leq n \leq N_t-1} \in \mathbb{R}$ and $(\beta^{[n]})_{0 \leq n \leq N_t-1}$, augmented by $\alpha^{[-1]} := \mathbf{1} \in \mathbb{R}^{N_u}$ and $\beta^{[-1]} := \mathbf{1} \in \mathbb{R}^{N_p}$, define for any $-1 \leq k \leq N_t - 1$ the quantities*

$$L_\alpha^{[k]} := \inf_{-1 \leq n \leq k} \left(\min_{1 \leq m \leq N_u} \left\{ \alpha_m^{[n]}, 0 \right\} \right), \quad R_\alpha^{[k]} := \sup_{-1 \leq n \leq k} \left(\max_{1 \leq m \leq N_u} \left\{ \alpha_m^{[n]}, 1 \right\} \right),$$

and, similarly, $L_\beta^{[k]}$ and $R_\beta^{[k]}$. Assume that $-\infty < L_\gamma^{[N_t-1]}$ and $R_\gamma^{[N_t-1]} < +\infty$, hold for $\gamma \in \{\alpha, \beta\}$, and that the Invariant Region Enforcing Condition (1.16) applies as

$$0 \leq \Delta_t^u \leq \frac{1}{\sqrt{3} \left(|L_\alpha^{[N_t-1]}| + |R_\alpha^{[N_t-1]}| \right)^2},$$

with similar conditions imposed on Δ_t^p .

Then, with either Neumann or Periodic boundary conditions, the sequence $U^{[k]}(X, \alpha^{[k]})$ and $P^{[k]}(\frac{1}{2} \cdot \mathbf{1}, \beta^{[k]})$ obtained using (2.16) remains bounded for all $0 \leq k \leq N_t$. More precisely, defining $M_\alpha^{[k]} := |L_\alpha^{[k]}| + |R_\alpha^{[k]}|$, for any $0 \leq k \leq N_t$ it holds that

$$\left(L_\alpha^{[k-1]} - \Delta_t^u M_\alpha^{[k-1]} \right) \mathbf{1} \leq U^{[k]}(X, \alpha^{[k]}) \leq \left(R_\alpha^{[k-1]} + \Delta_t^u M_\alpha^{[k-1]} \right) \mathbf{1}. \quad (2.17)$$

Similar bounds hold true for $P^{[k]}(\frac{1}{2} \cdot \mathbf{1}, \beta^{[k]})$, $L_\beta^{[k-1]}$, $R_\beta^{[k-1]}$, and $M_\beta^{[k-1]}$, Δ_t^p replacing, respectively, $U^{[k]}(X, \beta^{[k]})$, $L_\alpha^{[k-1]}$, $R_\alpha^{[k-1]}$, $M_\alpha^{[k-1]}$, and Δ_t^u in (2.17).

3. The PSBC applied on the MNIST database

We finally apply the PSBC model to several classification problems using the MNIST database. There are several hyperparameters that can be chosen in many different ways, a myriad of choices that we do not intend to exhaustively cover, let alone qualitatively study. Instead, we wish to understand how hyperparameters impact the model's accuracy, possibly degrading or improving it. Therefore no exhaustive search for their best combination was intended.

Four different aspects of the PSBC and its model compression qualities are investigated:

- (i) Different numbers of layers are considered: $N_t \in \{1, 2, 4\}$.
- (ii) Different layers- k -shared architectures are tested, for $k \in \{1, N_t\}$.
- (iii) Different parameterization cardinalities N_{pt} are considered, with $N_{pt} \in \{\lfloor \frac{784}{k} \rfloor, \text{ for } 1 \leq k \leq 5\}$.
- (iv) Different Boundary conditions, either Neumann or Periodic, are tested. Furthermore, the diffusion term is varied in $\varepsilon \in \{0\} \cup \{\frac{1}{2^k}, \text{ for } 0 \leq k \leq 4\}$. Boundary conditions are the same at $\varepsilon = 0$ (because no diffusion is present).

The methodology for model selection, model assessment, data preprocessing, and statistics are explained next. Further details about the MNIST database are found in the Appendix A.

Model selection and model assessment. Initially, the data set is split into train-development-test parts (Hastie et al., 2001, Chapter 7). Model selection is performed using 5-fold cross validations on the train-development set, where the hyperparameter with highest averaged accuracy is the one picked. Afterwards, with the chosen parameter in hands, we perform model assessment: the model is trained (again), but now on the whole train-development set. Accuracy is then measured on the test set which, up to this point, has been untouched by the model (Shalev-Shwartz and Ben-David, 2014, Chapter 11).

Data preprocessing and normalization. Preprocessing is necessary because MNIST images are 2D, but the PSBC requires a 1D initial condition. This is circumvented by flattening the images (i.e., writing them as column vectors), a procedural step also used in other models, like ANNs; see further discussion in Section 4.4.

Initially, preprocessing aims to fulfill the normalization conditions (1.7). But just this is insufficient, for MNIST images have a high number of pixels 0's and 1's, values that are stationary points under (1.6a). Thus, for each pair of distinct digits $(a, b) \in \{0, \dots, 9\}$ we use a normalization map of the form

$$\mathcal{N}_{(a,b)}(X) = 0.5\mathbf{1}_{N_u} + 0.5(X - \mu_{\text{training}}^{(a,b)}). \quad (3.1)$$

where $\mu_{\text{training}}^{(a,b)}$ represents the average of the training set associated with those same digits. The construction is designed in such a way that the statistical average over elements in the training set is $0.5\mathbf{1}_{N_u}$; the reason is because 0.5 is the average value of each weight during initialization. Furthermore, it holds that $\mathcal{N}_{(a,b)}([0, 1]^{N_u}) \subset [0, 1]^{N_u}$.

We remark that the normalization map depends on the pair of digits and the training sample only, remaining the same in different model assessments.

Statistics. For any given set of hyperparameters, models are fitted 5 times. This is done in order to assess statistical properties of the model, for weights are initialized in a randomized fashion. See initialization details in the Appendix A.

3.1 Results for the PSBC

We consider the PSBC with $\varepsilon = 0$, $N_t = 2$, and $N_{\text{pt}} = 196$, applied to 45 distinct pairs of digits (a, b) in $\{0, \dots, 9\}$, trained and tested on the subsets corresponding to those same digits. For each one of these digits, 5 PSBC models are fitted under the model selection and model assessment guidelines explained above. Statistics for each of these tests are shown in the Table 1.

| | 1 | 2 | 3 | 4 | 5 | 6 | 7 | 8 | 9 |
|---|-----------------------|-----------------------|------------------------|-----------------------|------------------------|-----------------------|-----------------------|-----------------------|-----------------------|
| 0 | 0.99 _(0.0) | 0.94 _(0.0) | 0.93 _(0.0) | 0.96 _(0.0) | 0.91 _(0.01) | 0.93 _(0.0) | 0.98 _(0.0) | 0.92 _(0.0) | 0.95 _(0.0) |
| 1 | | 0.95 _(0.0) | 0.96 _(0.0) | 0.96 _(0.0) | 0.94 _(0.0) | 0.97 _(0.0) | 0.95 _(0.0) | 0.94 _(0.0) | 0.97 _(0.0) |
| 2 | | | 0.92 _(0.01) | 0.97 _(0.0) | 0.95 _(0.0) | 0.95 _(0.0) | 0.96 _(0.0) | 0.94 _(0.0) | 0.96 _(0.0) |
| 3 | | | | 0.99 _(0.0) | 0.83 _(0.01) | 0.98 _(0.0) | 0.97 _(0.0) | 0.88 _(0.0) | 0.97 _(0.0) |
| 4 | | | | | 0.95 _(0.0) | 0.97 _(0.0) | 0.96 _(0.0) | 0.97 _(0.0) | 0.84 _(0.0) |
| 5 | | | | | | 0.95 _(0.0) | 0.96 _(0.0) | 0.92 _(0.0) | 0.95 _(0.0) |
| 6 | | | | | | | 0.99 _(0.0) | 0.98 _(0.0) | 0.99 _(0.0) |
| 7 | | | | | | | | 0.96 _(0.0) | 0.9 _(0.0) |
| 8 | | | | | | | | | 0.95 _(0.0) |

Table 1: Accuracies on test set (for the corresponding individuals associated with those labels). Parentheses values indicated standard deviation. Statistics consider 5 independent model assessments. Values were rounded to 2 digits.

Of the 45 cases, 3 have average in the range $[80\%, 90\%)$, 11 in the range $[90\%, 95\%)$, 31 in the range $[95\%, 100\%)$. A more detailed analysis of these classifiers is done with the help of confusion matrices, as carried out in the next section (after aggregation). In both scenarios the qualitative summary is the same: while for some pairs of digits the PSBC shows high accuracy with remarkably small number of false positives and false negatives, in other cases the results are simply poor. Obviously, one of the simplest ways to improve any of these models is by doing a more extensive grid search for hyperparameters (ours was in fact small, made up of about 100 different points). Instead, in Section 3.3 we go in a different direction, discussing how other ML techniques can be used to enhance the PSBC.

3.2 Constructing a multiclass classifier.

There are several possible approaches to generalize a binary classifier to a multiclass classifier. For illustration, we resort to combining classifiers by aggregation, followed by a *one versus one* technique (Hastie et al., 2001, Chapter 18.3.3). The binary classifiers used are those from Section 3.1, hence we continue with hyperparameters $\varepsilon = 0$, $N_t = 2$, and $N_{pt} = 196$.

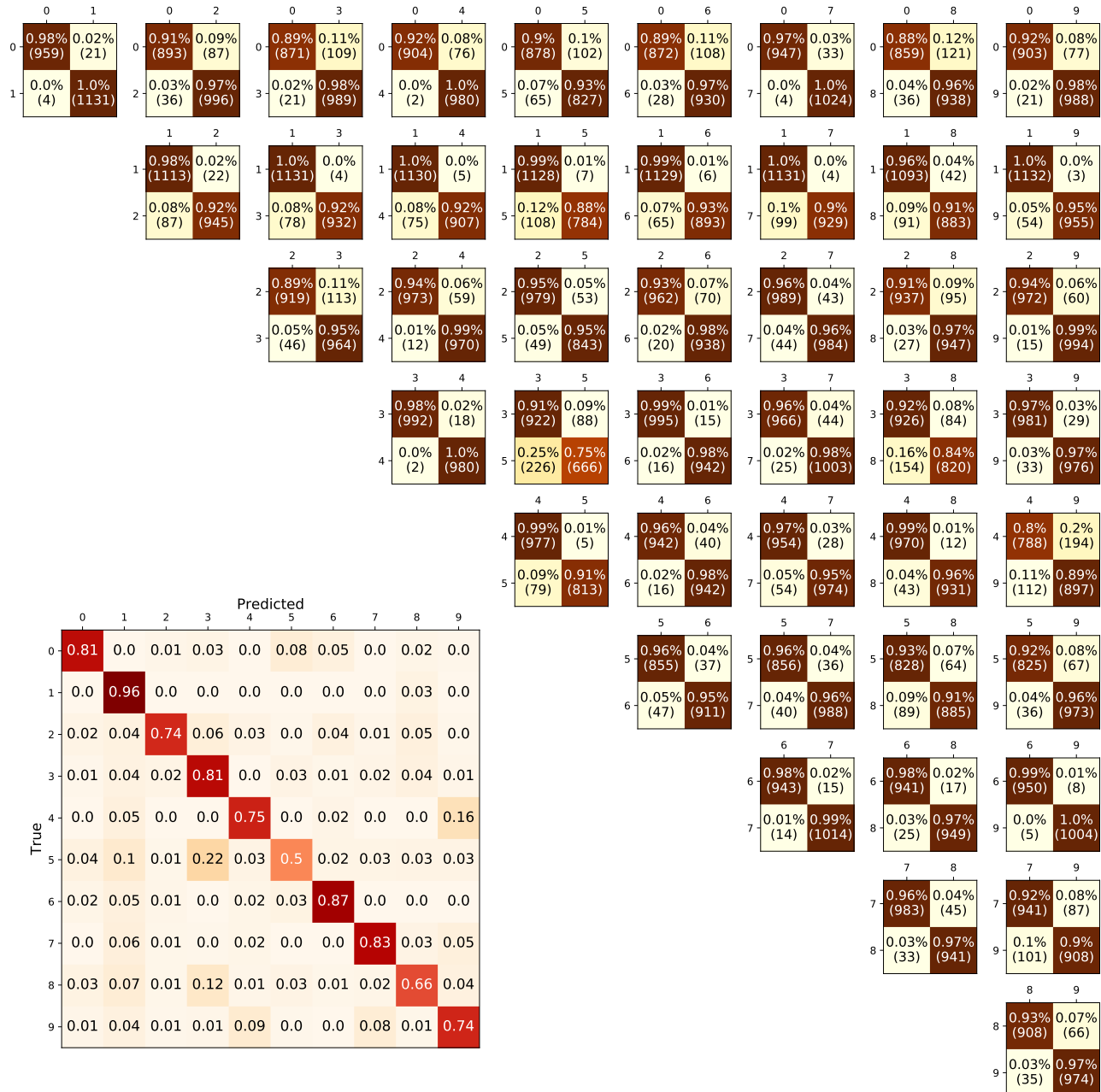


Figure 8: On the lower left, the confusion matrix of a multiclass classifier constructed with committees of PSBC (binary) classifiers (top, right). Each binary classifier’s parameters were $N_t = 2$, $N_{pt} = 196$, and $\varepsilon = 0$. Model selection is carried out by grid search for learning rates, Δ_t^p , Δ_t^u . The best chosen models is trained 5 times on the training-development set. Afterwards, a final classifier is constructed using Ensemble learning with hard-voting. Accuracy values on the test set are those displayed. Accuracy of the multiclass classifier is 77.25%. Values were rounded to 2 digits.

We finally turn to the construction of the multiclass classifier. Initially, for each distinct pair of digits $(a, b) \in \{0, \dots, 9\}$ we combine the 5 classifiers described in the previous section into a single classifier using Ensemble Learning principles with hard voting (Hastie et al., 2001, Chapters 8.7). The resulting classifier - which we denote by $\mathbb{P}_{(a,b)}(\cdot)$ - also has an associated map $\mathcal{N}_{(a,b)}(\cdot)$ constructed as in (3.1); observe that $\mathbb{P}_{(a,b)}(\cdot)$ varies over model assessments due to statistical variability of the classifiers, while $\mathcal{N}_{(a,b)}(\cdot)$ does not. Afterwards, multiclass prediction proceeds by majority voting.⁶

Results are shown in Figure 8. As one can see, the accuracy obtained on the test set is not high: 77.25% only. Evidently, there are many ways to improve this figure. For instance, one could begin by improving each one of these binary classifiers, whose accuracies vary considerably across different pairs of digits; some ideas are discussed and tested in Section 3.3. Another approach, one that takes the variability in classifiers' accuracies into account, pushes hard voting aside and assigns weights to voters instead; this can be achieved using Boosting methods (Hastie et al., 2001, Chapters 10 and 16).

3.3 Modeling the data manifold by changing the basis matrix.

As pointed out in Remark 2.6, an obvious way to improve the model is by allowing the basis matrices $\mathcal{B}^{\lfloor \cdot \rfloor}$ to vary over layers. Evidently, in light of Lemma 6(ii) such variations change the architecture of the network, distorting the approximation space where the prediction map is built.

Faced with many possible choices for basis matrices, some intuition about the role of trainable weights can be useful. During training, for example: in light of Lemma 10 ($N_u = 1$), one can conclude that Equation (1.6a) is hyperplane separating the set of initial conditions by proper adjustment in the values of $\alpha^{\lfloor \cdot \rfloor}$ (and, whenever necessary, fixing labels by changing $\beta^{\lfloor \cdot \rfloor}$). Even in a high-dimensional feature space we can still say that this is what is happening when canonical basis matrices are used (thanks for Lemma 6(ii)).

A less direct but maybe more interesting approach consists of modeling the basis matrix on the data manifold. We did some studies in this regard, combining the PSBC with Principal Components Analysis (PCA) (Hastie et al., 2001, Section 14.5). In this case, \mathcal{B}_u consists of the first N_{pt} principal components associated with the trained data, properly centered for such computations. As before, we take $\mathcal{B}_p = \text{Id}_{N_p}$, for a subordinate model ($N_p = N_{pt}$). Although the results improve those shown in Figure 8, the choice for \mathcal{B}_{sub} holds with less motivation, for it is still constructed in the canonical way described in Remark 7. The results displayed in Figure 9 are interesting, indicating that the lowest scores among False Positive and False Negatives increase, while the highest values among False Negatives and False Positives decay, making predictions using the PSBC with PCA more "balanced" than with the usual PSBC. In any case, these results are mostly illustrative, and more statistical evidence or theoretical understanding is required. Further technical details, mostly concerning the application of Invariant Region Enforcing Condition (1.16), are discussed in Section 3.5.

It must be said that when PCA is applied neither sparsity nor disjointness of basis elements' support (principal components) are expected, properties which imply model parallelization in the non-diffusive PSBC ($\varepsilon = 0$), according to Lemma 6(ii). In reality, and in spite of the results shown in this section, it is unclear what qualities sparse basis matrices offer to the PSBC. Nonetheless, it could be interesting to investigate the construction of basis matrices using techniques like Sparse Principal Components, with the caveat that Lasso methods foster sparsity, but not disjointness of basis' supports; cf (Hastie

6. In details, it goes as follows. First, individuals in the test set are min-max normalized to fit into the box $[0, 1]^{N_u}$. They are normalized again by $\mathcal{N}_{(a,b)}(\cdot)$ before classification using the model $\mathbb{P}_{(a,b)}(\cdot)$. Without loss of generality, we assume that, whenever $a < b$, a receives label 0, while b receives label 1. Then, all votes are computed as $\mathbb{M}_{(a,b)}(\cdot) = 1 - \mathbb{P}_{(a,b)}(\cdot)$ if $a < b$, $\mathbb{M}_{(a,b)}(\cdot) = \mathbb{P}_{(a,b)}(\cdot)$ if $b < a$, and zero otherwise. Afterwards, votes are counted as $\mathbb{C}_a(\cdot) = \sum_{b \neq a} \mathbb{M}_{(a,b)}(\cdot)$. The predicted label is assigned by sampling uniformly among individuals with highest score, so as to avoid ties; that is, sampling uniformly from $\{a | \mathbb{C}_a(X) = \max_{0 \leq \gamma \leq 9} \mathbb{C}_\gamma(X)\}$.

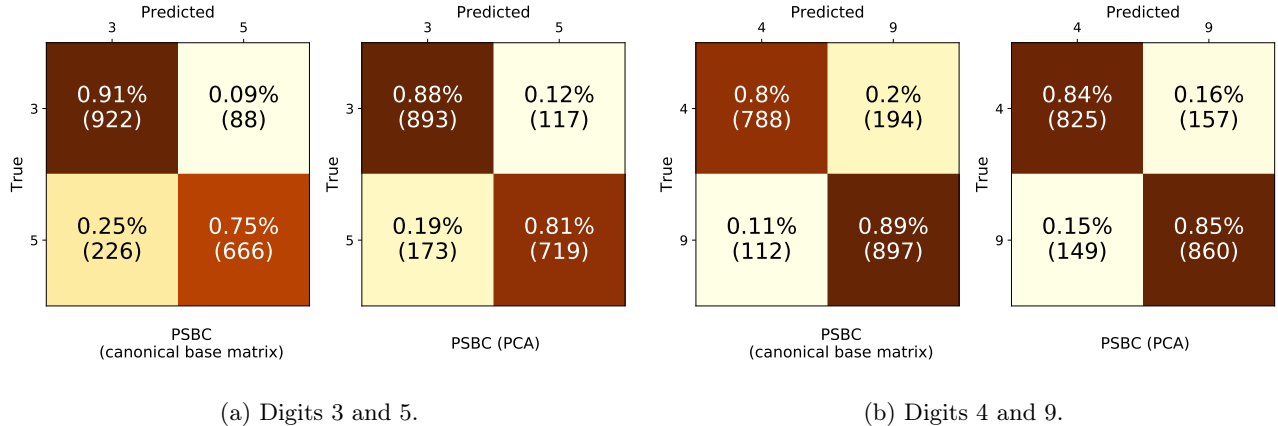


Figure 9: Confusion matrices comparing different models that were constructed using Ensemble Learning methods, with different base classifiers - PSBC models with canonical base matrix or PSBC models with base matrices built using PCA. The confusion matrix for digits 3 and 5 is shown in 9a, showing some improvement in accuracy, which goes from 83.49% to 84.75%, while F1 score jumps from 80.92% to 83.22%. On the other hand, the confusion matrix for digits 4 and 9 is shown in 9b, but in this case the result is mixed, and seems to deteriorate: accuracy remains the same (84.63%), while F1 scores shows a slight decrease, from 85.43% to 84.9%. Values were rounded to 2 digits.

et al., 2001, Section 14.5.5). If model parallelization is indeed necessary, this search can be converted into a combinatorial optimization problem.

3.4 Varying parameterization cardinality and viscosity rates — a study for the digits “0” and “1”.

As we explain below, model selection of hyperparameters was carried out considering that the model is computationally much cheaper at $\varepsilon = 0$, when no diffusion matrix multiplication is involved. For that reason we are specially interested in studying the impact of viscosity on model’s accuracy.

Evidently, different parametrization cardinalities yield different models, where a different number of weights are optimized. Nevertheless, with all hyperparameters fixed but ε , it is noteworthy that a non-diffusive ($\varepsilon = 0$) and a diffusive ($\varepsilon > 0$) models have the same number of trainable weights. Moreover, it is much cheaper and faster to train the first than the latter. Combining these facts, it seems interesting to investigate whether hyperparameters chosen through model selection in a non-diffusive setting ($\varepsilon = 0$) are still “good” hyperparameters for diffusive models ($\varepsilon > 0$), all other hyperparameters fixed. Does this model selection strategy yield improvement - or deterioration - of models’ accuracies?

With this question in mind, we apply model selection as follows: initially, hyperparameters N_t , N_{pt} , and layer- k -shared (for $k \in \{1, N_t\}$) are fixed. Grid search is carried out at $\varepsilon = 0$ for learning rates,⁷ Δ_t^u , and Δ_t^p ; they amount to 4 hyperparameters that are tuned through model selection, as explained earlier. The best hyperparameters are used for training the PSBC at all values of $\varepsilon \geq 0$ considered. In all the cases, model assessment (evaluation) uses the same training and test sets.

Figure 10 provides a comparison between the model’s behavior for different values of parameterization cardinality, as the diffusion term ε varies. Several observations are worthwhile mentioning.

First, the type of boundary condition does not seem to affect the model’s accuracy much. This is somehow expected due to flattening, but should not discourage further investigation, especially those generalizing the model to 2D features; see discussion in Sections 4.1 and 4.2. Second, that diffusion

7. Each set of weights in (1.6a) and (1.6b) allow for different learning rates.

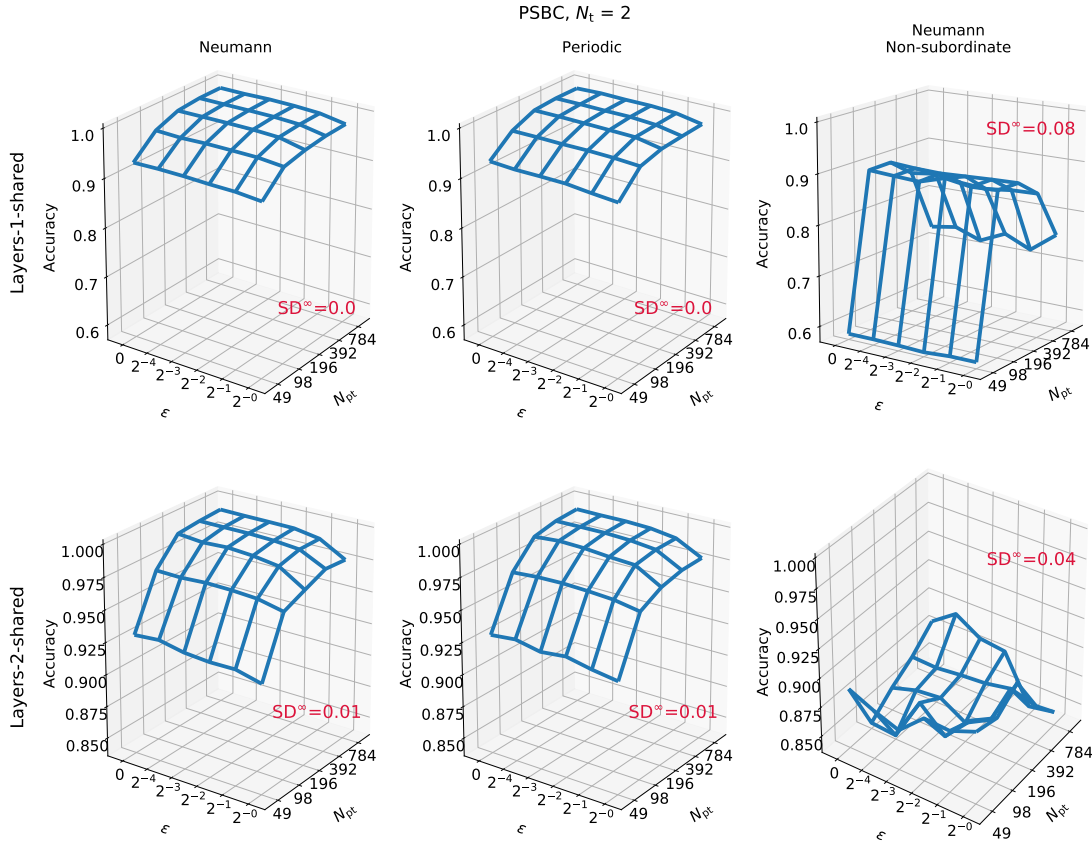


Figure 10: Accuracy for different values of viscosities ε and parameterization cardinalities N_{pt} . The classifier is applied to the “0” and “1” subset of the MNIST database. Each point on these surfaces is computed as an average of 5 experiments, with an associated standard deviation; SD^∞ indicates the largest among them. For convenience the positive part of the ε axis is in log-scale, whereas the N_{pt} axis is off scale, represented as an equally spaced grid. Values were rounded to 2 digits.

does not seem to improve the model trained at $\varepsilon = 0$, being in fact detrimental to accuracy in both cases - Neumann and Periodic boundary condition; on the other hand, diffusion seems to improve accuracy in some models with Neumann, non-subordinate architecture. Third and last, that in the case of Periodic and Neumann boundary conditions with high parameterization cardinality ($N_{pt} \approx N_u$), the cheapest PSBC with layers- N_t -shared architecture (all layers are shared) perform as well as a PSBC with layers-1-shared (more expensive for optimization). Surprisingly, in some cases the classifier achieves on average more than 90% accuracy even when $N_{pt} = 49$ the model, that is, with less than 100 variables (layers-2-shared), a remarkable manifestation of PSBC’s model compression qualities and an impossible milestone for ANNs with no weight sharing, where the minimum number of nodes is always bigger than the dimension of the input space.

Similar figures, for $N_t \in \{1, 4\}$, are available in the Supplementary Material.

3.5 The Invariant Region Enforcing Condition in practice.

It is important to study the behavior of trainable weights of optimized models. In Figure 11 we analyze how different boundary conditions, diffusion, and parameterization cardinality affects the sup

norm of the best models we obtained (whose accuracies are displayed in Figure 10 in some cases; see also the Supplementary Material).

We must emphasize that the interval $\mathcal{R}_\alpha^{\lfloor N_t-1 \rfloor} := \text{conv} \left(\{0, 1\} \cup_{m=0}^{N_t-1} \{\alpha^{\lfloor m \rfloor}\} \right)$ is built using elements on the range of the map (2.6). For this reason, when arbitrary basis matrices \mathcal{B}_u are used, $\mathcal{R}_\alpha^{\lfloor N_t-1 \rfloor}$ may not be easily recovered in terms of $W_u^{\lfloor \cdot \rfloor}$'s entries, making computations using the PSBC slightly more expensive. Luckily, that's not an issue when canonical basis matrices are used; in such case, according to Remark 7, we can rewrite

$$\mathcal{R}_\alpha^{\lfloor N_t-1 \rfloor} = \text{conv} \left(\{0, 1\} \cup_{m=0}^{N_t-1} \{W_u^{\lfloor m \rfloor}\} \right).$$

This property can be used to understand the ℓ^∞ -norm of weights, since

$$\max_{0 \leq n \leq N_t-1} \left\{ \|\alpha^{\lfloor n \rfloor}\|_{\ell^\infty}, 1 \right\} \leq \text{diam}(\mathcal{R}_\alpha^{\lfloor N_t-1 \rfloor}) \leq 2 \max_{0 \leq n \leq N_t-1} \left\{ \|\alpha^{\lfloor n \rfloor}\|_{\ell^\infty}, 1 \right\};$$

bounds in terms of $\|W_u^{\lfloor \cdot \rfloor}\|_{\ell^\infty}$ are immediate, thanks to Lemma 6(i). Similar statements are valid in the case of $\mathcal{R}_\beta^{\lfloor \cdot \rfloor}$, $\beta^{\lfloor \cdot \rfloor}$, and $W_p^{\lfloor \cdot \rfloor}$.

In Figure 11 we study the behavior of trainable weights attained at best accuracy (according to Early Stopping). It indicates that the diameters of $\mathcal{R}_\alpha^{\lfloor \cdot \rfloor}$ and $\mathcal{R}_\beta^{\lfloor \cdot \rfloor}$ grow at different rates, implying that Δ_t^u and Δ_t^p shrink towards zero with different rates in virtue of (1.16). In fact, this observation is in good agreement with our numerical experiments; see the Supplementary Material.

Earlier simulations on the MNIST database have shown that imposing the constraint $\Delta_t^u = \Delta_t^p$ in each epoch does not give good results. Furthermore, allowing Δ_t^u and Δ_t^p to assume their maximum value gives poor accuracy results, probably because in this way the model's hyperparameters vary too many times over different epochs. To circumvent such an issue, after each batch evaluation we use update Δ_t^u and Δ_t^p using the Invariant Region Enforcing Condition (1.16) in the form

$$\Delta_t^u := \min \left\{ \Delta_t^*, \frac{1}{\sqrt{3} \text{diameter} \left(\mathcal{R}_\alpha^{\lfloor N_t-1 \rfloor} \right)^2} \right\},$$

with a similar definition holding for Δ_t^p . Here, Δ_t^* indicates Δ_t^u 's initial value. Further information about parameters initialization can be found in the Appendix A.

4. Discussion, some extensions, and open questions

As we recall from Section 1, binary classification concerns the construction of approximations $\tilde{h}(\cdot)$ to an unknown hypothesis map $h(\cdot)$. Some of these methods can be motivated by biological mechanisms: for instance, the design and structure of CNNs bear similarity to how cortical neurons are scattered throughout the brain, while CNNs' functioning resemble cortical neurons orientation selectivity to visual stimuli. Likewise, the design of ANNs is reminiscent of the brain's networks (Goodfellow et al., 2016, Chapters 1 and 9.10). In regard to the PSBC, whenever $N_u = 1$ and $\varepsilon = 0$ its component (1.6a) can be interpreted as a discrete ODE modeling a nothing-or-all system, that is, a phenomenon of binary nature, which resembles neurons' reaction to stimuli: depending on a threshold (in this case, denoted by $\alpha(\cdot)$), stimuli are classified as inhibitory or excitatory. In terms of mathematical or physical modeling these resemblances are mostly metaphoric, even though, to the author's knowledge, likening binary classification to phase separation processes seems to be new.

Nonetheless, we have been inspired by many of these ideas (specially by those we oppose). First, by introducing a model that is not based on brain-like phenomena we just reiterate our belief that

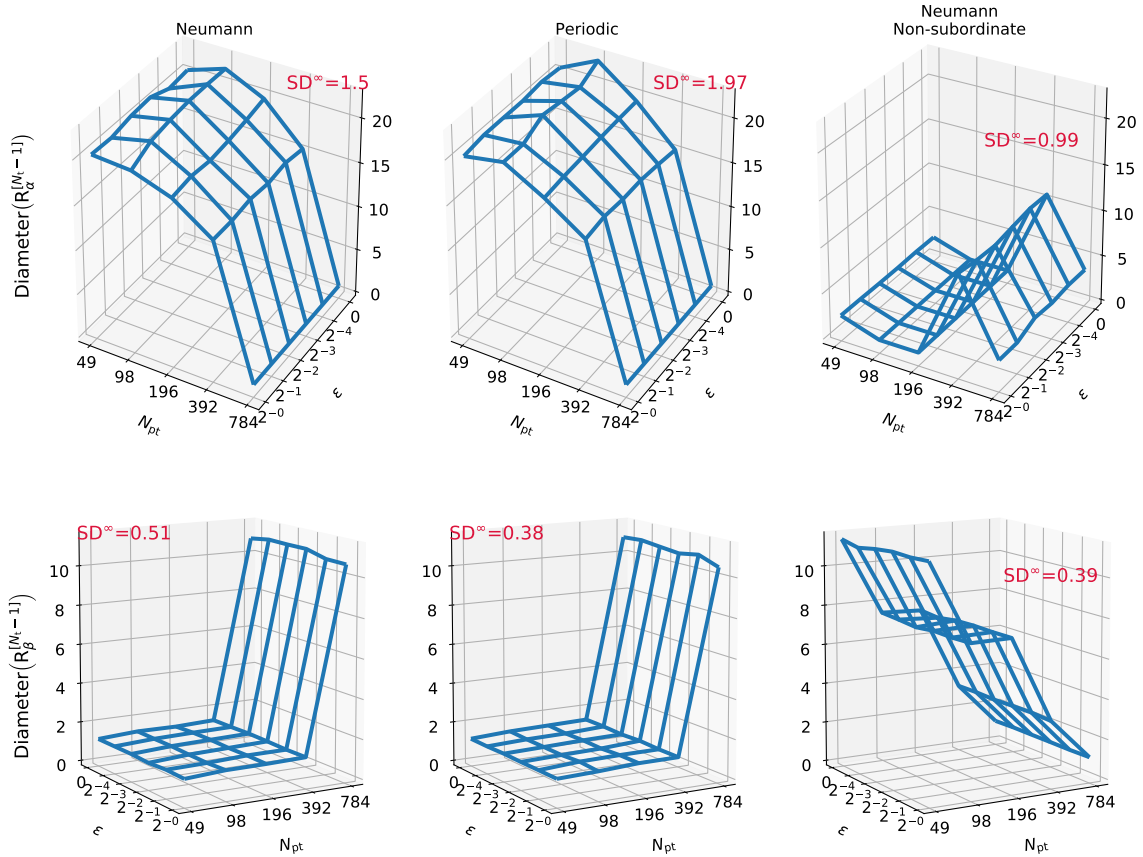
PSBC, $N_t = 2$, layers-1-shared


Figure 11: Average values attained by the diameter of the set $\mathcal{R}_\alpha^{[N_t-1]} := \text{conv}(\{0, 1\} \cup_{m=0}^{N_t-1} \{\alpha^{\lfloor m \rfloor}\})$ at the best epoch (according to an Early Stopping criterion); $\mathcal{R}_\beta^{[N_t-1]}$ is defined similarly. Different values of viscosities ε and parameterization cardinalities N_{pt} have been tested. The classifier is applied to the “0” and “1” subset of the MNIST database. Each point on these surfaces is computed as an average of 5 experiments, with an associated standard deviation; SD^∞ indicates the largest among them. For the time evolution of these diameters through epochs, see the figures in the Supplementary Material and also the accompanying movie file (Monteiro, 2021b, [Example_layers_snapshots.mp4](#), about 0.5 Mb). For convenience the positive part of the ε axis is in log-scale, whereas the N_{pt} axis is off scale, represented as an equally spaced grid. Values were rounded to 2 digits.

such quality is simply unnecessary. Second, by likening binary classification to the process of phase separation in binary fluids. Third, by likening stable (asymptotic) patterns in Reaction-Diffusion Equations to the process of labeling in supervised learning. Last, by showing that forward propagation can be done without squashing nonlinearities, turning it into an initial boundary value problem that is amenable to mathematical techniques from the field of PDEs.

In the sequel we make a few remarks concerning the PSBC. The topics addressed point out to directions in which the model can be improved, investigated, or extended in manners that we did not, at least in this first paper, exploited in depth.

4.1 On diffusion matrices and boundary conditions

Besides different boundary conditions, other modifications in the diffusion matrix can be envisioned if one observes that the matrix D_{N_u} represents a first-order accurate finite difference scheme for the operator ∂_x^2 (Strikwerda, 1989, Chapter 3). One could also consider finite difference schemes of higher order of accuracy, to which new diffusion matrices are associated.

We highlight that the matrix L_{N_u} in (2.12) is invertible for all $\varepsilon^2 \geq 0$ in both boundary condition cases, Neumann or Periodic. Hence, varying ε^2 is legitimate and does not affect the Invariant Region Enforcing Condition, which does not depend on ε . It is therefore plausible, at least in principle, that the parameter ε^2 could also be trained using backpropagation, in such a way that diffusion could be learned “on-the-fly”. Nonetheless, the diffusion matrices considered here - D_{N_u} and $D_{N_u}^{(\text{per})}$ - are too “rigid”, in the sense that they couple features with the same weights, regardless of their statistical correlation. It would be interesting to optimize the viscosity matrix as a trainable weight while keeping its negative semidefinite structure. This approach would generalize the periodic case studied here, and can be achieved by considering a Cholesky factorization of the diffusion as $D = -VV^T$ and optimizing for the entries in V .

4.2 Extending the PSBC using a multi-d diffusion operator

A deeper analysis of (2.13) indicates that the diffusion term ε controls the strength of interaction between features. This can be seen by a Neumann series expansion,

$$L_N^{-1} = (\text{Id}_N - \varepsilon^2 D_N)^{-1} = \sum_{n=0}^{\infty} \varepsilon^{2n} D_N^n,$$

which is valid for sufficiently small values of ε (Dym, 2007, Chapter 7.7, Lemma 7.15). One immediately concludes that L_N^{-1} is diagonal dominant. Moreover, due to the band-limited structure of D_N and its powers, it implies that elements of L_N^{-1} decay polynomially in ε the farther away from the diagonal they are.

The comments above lead us to a concerning conclusion: that the PSBC favors features interaction based on the proximity of their indexes. Flattening seems then unsatisfactory, in spite of high accuracy results obtained here. It should be noted that flattening does not affect models like ANNs due to their fully connected layers.

Removing the PSBC’s dependence on flattening is an important - and tangible - direction of improvement, which can be attained if one extends the model by changing (1.6a) to a multi-d spatial diffusion. Mathematically, this amounts to substituting the 1D Laplacian ∂_x^2 in (1.8) by a 2D Laplacian $\partial_x^2 + \partial_y^2$. As mentioned before, any discretization of the 2D Laplacian obeying the Maximum Principles as developed in Appendix B and C yields a model with similar mathematical properties - Invariant Regions, Invariant Region Enforcing Condition etc.

Overall, there is another reason for allowing more general diffusion matrices: learning boundary conditions rather than imposing them. Indeed, certain types of CNNs require padding of the input data with zeros, creating bias in the statistics close to the pictures’ edge (Goodfellow et al., 2016, Chapter 9.5). On the other hand, intuitively, it makes more sense to have boundary conditions that adapt statistical weights to features close to an edge.

It is plausible that a combination of a multidimensional diffusion model with the learning of general diffusion matrices (as discussed in Section 4.1) may not only result in better binary classifiers, but also in models that have considerable overlap with those developed and used in Computer Vision.

4.3 Invariant regions, growth of trainable weights in ℓ^∞ -norm, and the enforced invariant region condition

We have shown in Propositions 8, and 13 that $U^{[L]}$ and $P^{[L]}$ do not blow-up during forward propagation under appropriate assumptions. These results are important to the extent that they establish and secures one of the basic mechanisms used in the construction of the prediction map (1.5). Yet, there are many open questions about the asymptotic behavior of trainable weights. For instance, it is unclear whether an invariant region for trainable weights exists (in terms of hyperparameters and quantitative estimates on the data set \mathcal{S} used for its training). Overall, it is not known if either random initialization of trainable weights or the Invariant Region Enforcing Condition (1.16) are sufficient to ensure the existence of such an invariant region.

4.4 Comparison with other Machine Learning models

We have pointed out many similarities between the PSBC model and classical ones, like ANNs, CNNs, and RNNs. There are also some similarities when we compare the PSBC and CNNs. For instance, in the periodic case one can see the matrix L_N^{-1} as a Toeplitz matrix that plays the role of a convolution in (2.14) (Goodfellow et al., 2016, Chapter 9.1). The comparison becomes more explicit when we consider the fully explicit model (as in the Footnote 3),

$$U^{[n+1]} = \left(\text{Id}_{N_u} + \varepsilon^2 D_{N_u}^{(\text{per})} \right) U^{[n]} + \Delta_t^u f(U^{[n]}; \alpha^{[n]}), \quad (4.1)$$

where the matrix $\text{Id}_{N_u} + \varepsilon^2 D_{N_u}^{(\text{per})}$ has finite band and, when left multiplied with a column vector, acts as a convolution with a compact kernel. Unlike CNNs, the diffusive nature of these convolution kernels give them more physical motivation.

It is well known that the type of activation function has a huge impact in qualities of the model, its optimization, and mathematical properties concerning approximation theory (Goodfellow et al., 2016, Chapter 8). We highlight that the complexity of PSBC’s cost function on trainable weight, i.e., its polynomial degree, increases with N_t and N_{pt} , making high values of either (especially N_t) prohibitive. Such polynomial dependence however differs from - and contrasts with - standard ANN and CNN models, where activation functions introduce strong nonlinearities into the model.

| Sigmoid | $\sigma(z) = \tanh(z)$ | ReLU | PSBC, Eq. (2.15) |
|---|---|--|---|
| $\sigma(z) = \frac{1}{1+e^{-z}}$ | | $\sigma(z) = \max\{0, z\}$ | $\sigma(z = (u, w)) = f(u; w)$ |
| $\sigma(\mathbb{R})$ bounded | $\sigma(\mathbb{R})$ bounded | $\sigma(\mathbb{R})$ unbounded | $f(\mathbb{R}; w)$ unbounded |
| $\partial_z \sigma(\mathbb{R})$ bounded | $\partial_z \sigma(\mathbb{R})$ bounded | $\partial_z \sigma(\mathbb{R})$ bounded ⁸ | $\partial_u f(\mathbb{R}; w)$ unbounded |

Table 2: A few types of activation functions and some of their properties; cf. (Goodfellow et al., 2016, Chapters 6 and 9).

Several activation functions are described in Table 2, where properties of their 0th and 1st order derivatives - which differ substantially - are summarized. Indeed, both sigmoid and hyperbolic tangent activation functions are bounded, and their first order derivatives decay fast towards zero, making the learning process slow when trainable weights are too large; for these reasons they are sometimes called *squashing nonlinearities*. In contrast, the PSBC has polynomial activation functions. Activation functions of ReLU type differ because their (almost everywhere) derivatives are bounded, which is not necessarily the case for the PSBC.

Last, it must be said that the architecture of the PSBC bears similarities to (one to one) Recurrent Neural Networks (RNNs), especially in the case of the PSBC with layers- N_t -shared architecture, whose

7. Derivative in almost everywhere sense.

definition is recursive (from last layer down to input layer). Another point of similarity is that, in the PSBC construction, both Δ_t^p and Δ_t^u are fed to the model before forward propagation, like hidden parameters fed to an RNN’s initial layer; in such case, the fixed values Δ_t^p or Δ_t^u would be modified - or rather “distorted” - by weights after each backpropagation, and then propagate through the RNN network. But this analogy stops here: RNN’s weights are optimized with the sole intention of improving the model with respect to a cost function. In addition to that, the feature’s growth during forward propagation is tamed with squashing nonlinearities. Differently, in the PSBC both Δ_t^u and Δ_t^p are adjusted by the Invariant Region Enforcing Condition (1.16) to tame features’ growth during forward propagation; cf. (Goodfellow et al., 2016, Chapter 10, especially 10.7 and 10.8).

Supplementary Material, Data and Code availability

All the code for this paper has been written in Python and is available on Github (Monteiro, 2021b), which also contains Supplementary Material. Relevant data is available at “Monteiro (2021a)”.

Acknowledgments

The author would like to thank the hospitality of the Indiana University-Bloomington (U.S.A.), where he had several interesting conversations about gradient flows with Peter Sternberg.

Appendix

Appendix A. Initialization, optimization, hyperparameter tuning, and hardware

Hardware and computational statistics. To make replication and verification simpler, small computations were performed using Google Colab notebooks with TPUs. Unavoidably lengthier numerical computations (mostly related with training the model on the MNIST database) were performed on a supercomputer at MathAM-OIL using 6 cores over a single node.

MNIST database. This database consists of 70,000 images of handwritten digits from 0 to 9, each with size 28×28 pixels, stored as matrices of the same dimension. Following a historical trend in the ML field, the first 60,000 individuals were chosen for train-development purposes, while the last 10,000 individuals make up the test set. For further details, see “Lecun et al. (1998)”.

Initialization. Trainable weights $W_u^{[l,j]} \in \mathbb{R}^{N_{pt}}$ in (1.6a) and $W_p^{[l,j]} \in \mathbb{R}^{N_p}$ are initialized randomly, as Normal variables with mean 0.5 and diagonal covariance matrix, with variance σ^2 ; in all the simulations, we took $\sigma = 0.1$. Parameters Δ_t^u and Δ_t^p values contemplated during grid search were $\{0.1, 0.2\}$; although they have always been initialized with the same value, they evolve independently, as described in Section 3.5.

Optimization. We rely on several different optimization techniques.

Learning rates obey shrinking schedules, being discounted at a fixed rate every 5 epochs.

Model optimization uses (minibatches) Stochastic Gradient Descent (SGD), with minibatches of size 32. We do so due to limited computer memory, and also because adding noise to the parameter search (by subsampling the sample space) improves optimization. Minibatch size was chosen based on empirical studies pointing out that small size minibatches yield better performance (Masters and Luschi, 2018).

Number of epochs was 10 (grid search) and 20 (training), although optimization may stop earlier because *early stopping* was employed (Goodfellow et al., 2016, Chapter 7.8). In this way, weights are

recorded at their best value (according to a cost function being minimized), and optimization halts if the cost function does not achieve better results in the next p^* iterations; the quantity p^* receives the name *patience*. In all the simulations, Accuracy (1.2) was used as the monitored quantity. Patience was set as $p^* = 10$ in both grid search and training.

Appendix B. Some discrete maximum principles

The results in this section are all standard: they are discrete counterparts to classical results in elliptic PDE theory (Gilbarg and Trudinger, 1983, Chapter 3). We prove them here for the sake of completion, referring the reader to “(Strikwerda, 1989, Theorem 12.5.1)” for a different approach.

In what follows, let $V \in \mathbb{R}^N$, for $N \geq 3$. For any $j \in \{1, \dots, N\}$, define

$$\text{Average}_{\partial\{j\}}(V) := \begin{cases} V_2, & \text{if } j = 1; \\ \frac{V_{j-1} + V_{j+1}}{2}, & \text{if } 1 < j < N; \\ V_{N-1}, & \text{if } j = N. \end{cases} \quad (\text{B.1})$$

We begin by proving an auxiliary result:

Lemma 14 *Let $V \in E = \mathbb{R}^N$. Consider D_N be the diffusion finite difference matrix as in (2.13). Then the following statements are true:*

(i) *The condition $(D_N V)_j \leq 0$ is equivalent to $\text{Average}_{\partial\{j\}}(V) \leq V_j$.*

(ii) *The condition $(D_N V)_j \geq 0$ is equivalent to $\text{Average}_{\partial\{j\}}(V) \geq V_j$.*

(iii) *If $V_m = \min_{1 \leq j \leq N} \{V_j\}$, then $(D_N V)_m \geq 0$. Likewise, if $V_M = \max_{1 \leq j \leq N} \{V_j\}$, then $(D_N V)_M \leq 0$.*

(iv) *(Invariant positive cone) Given $U \in \mathbb{R}_+^N$ and $\alpha \geq 0$ then $(\text{Id}_N - \alpha D_N)^{-1} U \in \mathbb{R}_+^N$.*

(v) $\|(\text{Id}_N - \alpha D_N)^{-1}\|_{\ell^\infty \rightarrow \ell^\infty} \leq 1$.

The results (iv) and (v) are important in the study of invariant regions (Hoff, 1978, Lemma 3.2.): the former is related to elliptic maximum principles, whereas the latter to parabolic maximum principles.

Proof. The proofs of (i)-(ii) are straightforward, hence omitted. Assertion (iii) is a direct consequence of (i) and (ii). We then prove (iv), arguing by contradiction. Assume the existence of $V \in \mathbb{R}_+^N \neq \mathbf{0}$ such that

$$(\text{Id}_N - \alpha D_N)^{-1} U \notin \mathbb{R}_+^N.$$

Taking $j = \text{argmin}(U)$, it must hold that $\{(\text{Id}_N - \alpha D_N)^{-1} U\}_j = U_j < 0$.

Now, let's rewrite the last equality in the equivalent form $V_j = \{(\text{Id}_N - \alpha D_N)U\}_j$. As $V \in \mathbb{R}_+^N$ the right hand side is non-negative, which implies that $(\alpha D_N U)_j \leq U_j < 0$. However, (iii) implies that $(D_N U)_j \geq 0$. This contradiction finishes the proof.

The proof of (v) is also by contradiction. Assume that $\|(\text{Id}_N - \alpha D_N)^{-1}\|_{\ell^\infty \rightarrow \ell^\infty} > 1$. Hence, there exist two vectors $V, U \in E$ such that $\|U\|_{\ell^\infty} = 1$, $\|V\|_{\ell^\infty} > 1$ and $(\text{Id}_N - \alpha D_N)^{-1} U = V$. Without loss of generality, let $M = \text{argmax}(V)$ be so that $V_M = \|V\|_{\ell^\infty} > 1$. Then, using (i), we get that $(D_N V)_M \leq 0$. On the other hand, we combine $\alpha \geq 0$ with $U = (\text{Id}_N - \alpha D_N) V$ to get

$$U_M = ((\text{Id}_N - \alpha D_N) V)_M = V_M - \alpha (D_N V)_M \geq V_M > 1,$$

in contradiction with $\|U\|_{\ell^\infty} = 1$. This finishes the proof of (v). ■

Remark 15 (Periodic Boundary Conditions) *The proofs in this session rely essentially on the Maximum Principle. They extend naturally to the case of periodic boundary conditions, substituting D_N in Lemma 14 by $D_N^{(\text{per})}$ given in 4.1 and modifying the average operator B.1 to*

$$\widetilde{\text{Average}}_{\partial\{j\}}(V) := \begin{cases} \frac{V_2+V_N}{2}, & \text{if } j = 1; \\ \frac{V_{j-1}+V_{j+1}}{2}, & \text{if } 1 < j < N; \\ \frac{V_{N-1}+V_1}{2}, & \text{if } j = N. \end{cases} \quad (\text{B.2})$$

Appendix C. Proofs and auxiliary results

Throughout this section we shall use the following notation: for any $p \in \mathbb{R}$ and any set $\mathcal{A} \subset \mathbb{R}$, define

$$\text{dist}(p, \mathcal{A}) := \inf_{q \in \mathcal{A}} |p - q|, \quad \text{and} \quad \text{diam}(\mathcal{A}) := \sup_{a, b \in \mathcal{A}} |a - b|.$$

Recalling the notion of convexity from Section 1.3, whenever a set \mathcal{A} is convex it is easy to show that for any two points p and q in it and any $C > 0$, we have

$$\text{dist}(p, \mathcal{A}) \leq C, \quad \text{and} \quad \text{dist}(q, \mathcal{A}) \leq C, \quad \text{implies} \quad \text{dist}(\lambda p + (1 - \lambda)q, \mathcal{A}) \leq C, \quad (\text{C.1})$$

therefore the set $\widetilde{\mathcal{A}} = \{p \in \mathbb{R} \mid \text{dist}(p, \mathcal{A}) \leq C\}$ is also a convex set.

C.1 An abstract invariant region lemma

Throughout the training process it is important to control the ℓ^∞ norm of trainable weights. Thanks to (1.4), we approach this problem by showing global existence⁹ of the dynamics (1.6), proving that $\|U^{[\cdot]}(X, \alpha^{[\cdot]})\|_{\ell^\infty}$ and $\|P^{[\cdot]}(\frac{1}{2}, \beta^{[\cdot]})\|_{\ell^\infty}$ can both be controlled by the ℓ^∞ -norm of the trainable weights $\alpha^{[\cdot]}$ and $\beta^{[\cdot]}$, independently of N_t .

As trainable weights $\alpha^{[\cdot]}$ and $\beta^{[\cdot]}$ vary throughout optimization, we need to understand how they affect the growth of $U^{[\cdot]}(X, \alpha^{[\cdot]})$ and $P^{[\cdot]}(\frac{1}{2}, \beta^{[\cdot]})$ as the latter propagate through (1.6a) and (1.6b), respectively. Roughly speaking, we understand the range of values that each of these quantities may assume by dividing them in two parts: one that is the convex hull of the trainable weights $\alpha^{[\cdot]}$ and $\beta^{[\cdot]}$, the other as an ‘‘spill out’’ region, whose existence is a side effect of numerical discretization.

We begin with an auxiliary result.

Lemma 16 *The polynomial $p(z) = -z^4 + z^3 + 2z - 1$ is non-negative in the range $1 \leq z \leq 1 + \frac{1}{\sqrt{3}}$.*

Proof. Rewrite the polynomial as $p(z) = z - (1 - z)^2(z^2 + z + 1)$. Then the result follows from $p(z) \geq z - \frac{(z^2+z+1)}{3} =: q(z) \geq q(1) = 0$ in $1 \leq z \leq 1 + \frac{1}{\sqrt{3}}$. ■

The next result is fundamental in the rest of this Appendix.

Lemma 17 (Abstract invariant region) *Let $\mathcal{R} \subset \mathbb{R}$ be a convex set of parameters satisfying $\{0, 1\} \subset \mathcal{R}$. For a fixed $\beta \in \mathcal{R}$, let*

$$U^{[n+1]} = U^{[n]} + \Delta_t U^{[n]}(1 - U^{[n]})(U^{[n]} - \beta). \quad (\text{C.2})$$

Then, the following properties hold:

9. We keep the term ‘‘global’’ even when $N_t < \infty$, because the result is easily extended to the case $N_t = +\infty$. Furthermore, because $\text{dist}(p, \mathcal{R}) = \text{dist}(p, \overline{\mathcal{R}})$ in the $\ell^\infty(\mathbb{R})$ topology, the result in Lemma 17 still holds when $\mathcal{S}^{[N_t]}$ has infinitely many points.

(i) If $U^{[n]} \in \mathcal{R}$, then $\text{dist}(U^{[n+1]}, \mathcal{R}) \leq \Delta_t \text{diam}(\mathcal{R})^3$.

(ii) For any $0 \leq \Delta_t \leq \frac{1}{\sqrt{3} \text{diam}(\mathcal{R})^2}$, the set $\mathcal{S} := \left\{ X \in \mathbb{R} \mid \text{dist}(X, \mathcal{R}) \leq \Delta_t \text{diam}(\mathcal{R})^3 \right\}$ is convex and positively invariant under (C.2).

We remark that when compared to classical global existence results in PDEs, Lemma 17(i) and Lemma 17(ii) are, roughly speaking, equivalent to showing local existence (and associated bounds), and then applying a bootstrap argument, respectively; cf. (Rauch and Smoller, 1978, Theorems 2.1 and 3.9).

Proof. [of Lemma 17] Throughout the proof we write $D = \text{diam}(\mathcal{R})$. To begin with, (C.2) gives

$$|U^{[n+1]} - U^{[n]}| = \Delta_t |U^{[n]}| \cdot |1 - U^{[n]}| \cdot |U^{[n]} - \beta|. \quad (\text{C.3})$$

Because $\{0, 1, \beta, U^{[n]}\} \subset \mathcal{R}$ we can majorize the right hand side by $\Delta_t D^3$. As $U^{[n]} \in \mathcal{R}$, the left hand side is bounded from below by $\text{dist}(U^{[n+1]}, \mathcal{R})$, and this completes the proof.

Now we turn to the proof of (ii). We prove positive invariance using an induction argument on n . The result is clearly true for $n = 0$, since $U^{[0]} = X \in \mathcal{S}$ due to the normalization condition (1.7). Thus, assuming that $U^{[k]} \in \mathcal{S}$ for all $0 \leq k \leq n$, we must prove that $U^{[n+1]} \in \mathcal{S}$.

A simplification is readily available: it suffices to consider the case $U^{[n]} \in \mathcal{S} \setminus \mathcal{R}$, for (i) contemplates the other case. To begin with, observe that \mathcal{S} is convex, which it inherits from the convexity of the set \mathcal{R} allied to convexity of the ℓ^∞ norm (see discussion below (C.1)). Thus, from $0 \in \mathcal{R} \subset \mathcal{S}$ we conclude that $\{-\Delta_t D^3, +\Delta_t D^3\} \subset \mathcal{S}$. Furthermore, as we also have that $U^{[n]} \in \mathcal{S}$, the result follows if we show that $U^{[n+1]}$ belongs to the interval $[-\Delta_t D^3, U^{[n]}]$ when $U^{[n]} \geq 0$, or that $U^{[n+1]}$ belongs to the interval $[U^{[n]}, +\Delta_t D^3]$ when $U^{[n]} \leq 0$. We shall prove only the former assertion, the proof of the latter being similar.

Since $U^{[n]} \in \mathcal{S} \setminus \mathcal{R} \subset \mathbb{R}$ is non-negative, we must have $U^{[n]} \geq \max\{1, \beta\}$ and, consequently, that $\Delta_t U^{[n]}(1 - U^{[n]})(U^{[n]} - \beta) \leq 0$; inspecting (C.2), this implies that $U^{[n+1]} \leq U^{[n]}$. Therefore, in order to finalize the proof it suffices to show that $-\Delta_t D^3 \leq U^{[n+1]}$ or, equivalently, that

$$-\Delta_t D^3 \leq U^{[n]} \left(1 + \Delta_t(1 - U^{[n]})(U^{[n]} - \beta) \right) \quad (\text{C.4})$$

holds, where the equivalence is due to (C.2). Since $U^{[n]}$ and $U^{[n+1]}$ have the same sign, it holds that $0 \leq U^{[n+1]} \leq U^{[n]}$, therefore both 0 and $U^{[n]}$ belong to the convex set \mathcal{S} . Consequently, we only need to consider the cases in which both quantities $U^{[n]}$ and $U^{[n+1]}$ have different signs.

It is easy to conclude by triangle inequality that $\text{dist}(U^{[n]}, p) \leq \text{dist}(U^{[n]}, q) + \text{diam}(\mathcal{R})$ for any $p, q \in \mathcal{R}$. By optimization on q and the induction hypothesis, this yields

$$\text{dist}(U^{[n]}, p) \leq \text{dist}(U^{[n]}, \mathcal{R}) + \text{diam}(\mathcal{R}) \leq D(1 + \Delta_t D^2).$$

Thus, we can bound $(1 + \Delta_t(1 - U^{[n]})(U^{[n]} - \beta))$ from below by $(1 - \Delta_t(D + \Delta_t D^3)^2)$, since $\{1, \beta\} \subset \mathcal{R}$. Consequently,

$$\min \left\{ (D + \Delta_t D^3) (1 - \Delta_t(D + \Delta_t D^3)^2), 0 \right\} \leq U^{[n]} \left(1 + \Delta_t(1 - U^{[n]})(U^{[n]} - \beta) \right).$$

It is evident that $-\Delta_t D^3 \leq 0$, therefore it suffices to study the values of Δ_t for which the inequality

$$-\Delta_t D^3 \leq (D + \Delta_t D^3) (1 - \Delta_t(D + \Delta_t D^3)^2),$$

holds, which we claim to hold whenever $\Delta_t D^2 \leq \frac{1}{\sqrt{3}}$ is satisfied. Indeed, we shall use a rearrangement of the above inequality as

$$-\Delta_t D^2 \leq (1 + \Delta_t D^2) (1 - \Delta_t D^2(1 + \Delta_t D^2)^2).$$

Plugging $Z = 1 + \Delta_t D^2$ into the previous inequality and expanding gives $-Z^4 + Z^3 + 2Z - 1 \geq 0$, which holds in the range $1 \leq Z \leq 1 + \frac{1}{\sqrt{3}}$, thanks to the result of Lemma 16. Unpacking, it gives the equivalent statement $\Delta_t D^2 \leq \frac{1}{\sqrt{3}}$, proving the claim. We have then established (C.4), and with this we conclude the proof. \blacksquare

Corollary 18 *For any sequence $(\alpha^{[k]})_{-1 \leq k \leq N_t - 1}$, with $\alpha^{[-1]} = 1$, define the sets*

$$\mathcal{R}^{[k]} := \text{conv} \left(\{0, 1\} \cup_{m=-1}^k \{\alpha^{[m]}\} \right),$$

for $-1 \leq k \leq N_t - 1$. Let $U^{[k+1]} = U^{[k]} + \Delta_t U^{[k]}(1 - U^{[k]})(U^{[k]} - \alpha^{[k]})$, with $U^{[0]} \in [0, 1]$, and $0 \leq k \leq N_t - 1$. Then, whenever $0 \leq \Delta_t \leq \frac{1}{\sqrt{3} \text{diam}(\mathcal{R}^{[N_t-1]})^2}$, we have

$$\text{dist}(U^{[k]}, \mathcal{R}^{[k-1]}) \leq \Delta_t \text{diam} \left(\mathcal{R}^{[k-1]} \right)^3, \quad \text{for all } 0 \leq k \leq N_t.$$

Remark 19 (the case of parameter range on a symmetric set) *In the case of \mathcal{R}_{sym} being a symmetric set about the origin (that is, $\beta \in \mathcal{R}_{\text{sym}}$ if and only if $-\beta \in \mathcal{R}_{\text{sym}}$), then it is possible to extend the previous proof to show that, whenever $0 \leq \Delta_t \leq \frac{1}{\text{diam}(\mathcal{R}_{\text{sym}})^2}$, the set*

$$\mathcal{S} := \left\{ X \in \mathbb{R} \mid \text{dist}(X, \mathcal{R}_{\text{sym}}) \leq \frac{\Delta_t}{2} \text{diam}(\mathcal{R}_{\text{sym}})^3 \right\}$$

is convex and positively invariant through (C.2). In such a case, Corollary 18 applies to $\mathcal{R}_{\text{sym}}^{[k]} := \text{conv} \left(\{0, 1, -1\} \cup_{m=-1}^k \{\alpha^{[m]}\} \cup_{m=-1}^k \{-\alpha^{[m]}\} \right)$.

C.2 Proof of results in Section 2

Proof. [of Proposition 8] It suffices to prove the 1D case ($N_u = 1$), since the dynamics is decoupled for each index, and the infimum (resp., supremum) of a quantity U_m over two sets $A \subset B$ is so that $\inf_{m \in B} U_m \leq \inf_{m \in A} U_m$ (resp., $\sup_{m \in B} U_m \geq \sup_{m \in A} U_m$).

For $\mathcal{R}^{[k]}$ as in Corollary 18, define

$$\mathcal{S}^{[k]} := \left\{ X \in \mathbb{R} \mid \text{dist}(X, \mathcal{R}^{[k]}) \leq \Delta_t^u \text{diam} \left(\mathcal{R}^{[k]} \right)^3 \right\}.$$

The equivalence between the interval $\left[L^{[k]} - \Delta_t^u M^{[k]}, R^{[k]} + \Delta_t^u M^{[k]} \right]$ and the set $\mathcal{S}^{[k]}$ is clear. Applying Corollary 18 then gives the result. \blacksquare

Proof. [of Lemma 10] We argue by contradiction. Assume that $U^{[j]}(X; \alpha^{[j]}) \geq U^{[j]}(\tilde{X}; \alpha^{[j]})$ holds for all $j \in \{0, \dots, n\}$ but at $n+1 \leq N_t$ we get for the first time

$$U^{[n+1]}(X; \alpha^{[n+1]}) < U^{[n+1]}(\tilde{X}; \alpha^{[n+1]}). \quad (\text{C.5})$$

From Proposition 8, we immediately obtain the bound $|U^{[n]}| \leq 1 + \Delta_t^u$, for all $n \in \{0, \dots, N_t\}$. Now, as $\alpha^{[n]} \in [0, 1]$ and $0 \leq \Delta_t^u \leq \frac{1}{10}$, a straightforward computation shows that

$$\max_{|U| \leq 2, \alpha \in [0, 1]} \left| D_U f(U, \alpha^{[n]}) \right| \leq 8 \left(1 + \frac{\Delta_t^u}{2} \right)^2 \leq 9. \quad (\text{C.6})$$

Using (2.1), a simple application of the Intermediate Value Theorem gives

$$\begin{aligned} U^{[n+1]}(X, \alpha^{[n+1]}) - U^{[n+1]}(\tilde{X}, \alpha^{[n+1]}) &= U^{[n]}(X, \alpha^{[n]}) - U^{[n]}(\tilde{X}, \alpha^{[n]}) \\ &\quad + \Delta_t^u(D_U f)\left(\theta, \alpha^{[n]}\right)\left(U^{[n]}(X, \alpha^{[n]}) - U^{[n]}(\tilde{X}, \alpha^{[n]})\right). \end{aligned}$$

for some $U^{[n]}(\tilde{X}, \alpha^{[n]}) \leq \theta \leq U^{[n]}(X, \alpha^{[n]})$. From (C.5) we conclude that the left hand side of the above equality is strictly negative. However, the bound in (C.6) and the assumption $0 \leq \Delta_t^u \leq \frac{1}{10}$ imply that the right hand side is non-negative. This contradiction implies that (C.5) cannot happen, and the result is therefore established. \blacksquare

Proof. [of Proposition 13] The proof is essentially a reprise of that in Lemma 17, with some subtle changes due to the presence of the diffusion operator; the main argument invokes Lemma 14(iv), an idea we learned from (Hoff, 1978, Theorem 3.3).

To begin with, observe that there is no diffusion in the component $P^{[k]}(\frac{1}{2}, \beta^{[k]})$, hence the proof of this case is contemplated by Corollary 9. Therefore, in the rest of the proof we are left with estimates for the component $U^{[k]}(X, \alpha^{[k]})$ only. For all $-1 \leq n \leq N_t - 1$, define

$$\underline{\gamma}^{[n]} := L_\alpha^{[n]} - \Delta_t^u M^{[n]}, \quad \bar{\gamma}^{[n]} := R_\alpha^{[n]} + \Delta_t^u M^{[n]}.$$

We have to show that $\underline{\gamma}^{[n]}\mathbf{1} \leq U^{[n+1]} \leq \bar{\gamma}^{[n]}\mathbf{1}$ holds for every $0 \leq n+1 \leq N_t$. First, we rewrite (1.6a) in its vectorial form (2.14) as a two-step model,

$$V^{[n+1]} = U^{[n]} + \Delta_t^u f(U^{[n]}; \alpha^{[n]}), \quad \text{and} \quad U^{[n+1]} = L_{N_u}^{-1} \cdot V^{[n+1]}. \quad (\text{C.7})$$

From here on we resort to an induction argument on n . The result is clearly true for $n = 0$, because of the normalization conditions (1.7). Hence, assume that the result holds for all $0 \leq j \leq n$.

Recall from (2.13) that $L_{N_u} = \text{Id}_{N_u} - \varepsilon^2 D_{N_u}$. Direct inspection shows that, for all $\gamma \in \mathbb{R}$,

$$L_N \cdot (\gamma\mathbf{1}) = \gamma\mathbf{1}, \quad \text{and} \quad (L_N)^{-1} \cdot (\gamma\mathbf{1}) = \gamma\mathbf{1} \quad (\text{C.8})$$

hold, since $D_N\mathbf{1} = 0$ regardless of the boundary conditions, Neumann or Periodic. In other words, the vector $\gamma\mathbf{1}$ is an eigenvector to $(L_{N_u})^{-1}$, with associated eigenvalue 1.

Now, because of the Invariant Region Enforcing Condition (1.16) we can apply the Corollary 9 to the first equation in (C.7), obtaining $\underline{\gamma}^{[n]}\mathbf{1} \leq V^{[n+1]} \leq \bar{\gamma}^{[n]}\mathbf{1}$. In other words, it holds that

$$V^{[n+1]} - \underline{\gamma}^{[n]}\mathbf{1} \geq 0, \quad \text{and} \quad \bar{\gamma}^{[n]}\mathbf{1} - V^{[n+1]} \geq 0.$$

Now, a left multiplication by $L_{N_u}^{-1}$ preserves these inequalities, thanks to invariance of the positive cone in Lemma 14(iv), yielding

$$L_{N_u}^{-1}\left(V^{[n+1]} - \underline{\gamma}^{[n]}\mathbf{1}\right) \geq 0, \quad \text{and} \quad L_{N_u}^{-1}\left(\bar{\gamma}^{[n]}\mathbf{1} - V^{[n+1]}\right) \geq 0.$$

Finally, we rewrite the first term using (C.7) and apply (C.8) to the second one, obtaining the desired inequalities. This completes the induction argument, concluding the proof. \blacksquare

Remark 20 (Continuum versus discrete) *It is important to contrast the techniques we use and those of the Invariant region theory, mostly applied in the continuum setting (Chueh et al., 1977). In the sequel, assume that $\partial_t v = F(v)$ represents a reaction-diffusion PDE, and $v_{n+1} = \tilde{F}(v_n)$ its discretization. Roughly speaking, the (continuum) theory looks for sufficient conditions on a set Ω and on the behavior of $F|_{\partial\Omega}(\cdot)$, in such a way that initial conditions for the Cauchy problem that start on*

Ω remain on it for all $t \geq 0$. Notably, none of these conditions directly apply to the discrete problem, but have been adapted in some cases (Hoff, 1978).

In showing that forward propagation is well-defined our goals are the same as those in the continuum theory: we prove that obstructive conditions prevent solutions to leave a certain bounded set (which is analogous to the aforementioned set Ω). Thus, the results of Propositions 8 and 13, and that of (Hoff, 1978, Theorem 3.3) are equivalent, although (i) we put emphasis on how the meshgrid Δ_t must be changed in order to enforce the existence of an invariant region and (ii), the techniques employed in part of the proofs differ. We highlight that we have the advantage of knowing both the range of initial conditions (due to the Normalization Condition 1.7) and the structure of the reaction term; thus, in scope, the result in “Hoff (1978)” applies to a wider range of reaction diffusion models.

References

- S. B. Angenent, J. Mallet-Paret, and L. A. Peletier. Stable transition layers in a semilinear boundary value problem. *J. Differential Equations*, 67(2):212–242, 1987. ISSN 0022-0396. doi: 10.1016/0022-0396(87)90147-1. URL [https://doi.org/10.1016/0022-0396\(87\)90147-1](https://doi.org/10.1016/0022-0396(87)90147-1).
- José A Carrillo, Robert J McCann, and Cédric Villani. Contractions in the 2-wasserstein length space and thermalization of granular media. *Archive for Rational Mechanics and Analysis*, 179(2):217–263, 2006.
- Richard G. Casten and Charles J. Holland. Instability results for reaction diffusion equations with Neumann boundary conditions. *J. Differential Equations*, 27(2):266–273, 1978. ISSN 0022-0396. doi: 10.1016/0022-0396(78)90033-5. URL [https://doi.org/10.1016/0022-0396\(78\)90033-5](https://doi.org/10.1016/0022-0396(78)90033-5).
- Nathaniel Chafee. Asymptotic behavior for solutions of a one-dimensional parabolic equation with homogeneous Neumann boundary conditions. *J. Differential Equations*, 18:111–134, 1975. ISSN 0022-0396. doi: 10.1016/0022-0396(75)90084-4. URL [https://doi.org/10.1016/0022-0396\(75\)90084-4](https://doi.org/10.1016/0022-0396(75)90084-4).
- K. N. Chueh, C. C. Conley, and J. A. Smoller. Positively invariant regions for systems of nonlinear diffusion equations. *Indiana Univ. Math. J.*, 26(2):373–392, 1977. ISSN 0022-2518. doi: 10.1512/iumj.1977.26.26029. URL <https://doi.org/10.1512/iumj.1977.26.26029>.
- Felipe Cucker and Steve Smale. On the mathematical foundations of learning. *Bulletin of the American mathematical society*, 39(1):1–49, 2002.
- Mark R. Dennis, Paul Glendinning, Paul A. Martin, Fadil Santosa, and Jared Tanner, editors. *The Princeton companion to applied mathematics*. Princeton University Press, Princeton, NJ, 2015. ISBN 978-0-691-15039-0. doi: 10.1515/9781400874477. URL <https://doi.org/10.1515/9781400874477>.
- Luc Devroye, László Györfi, and Gábor Lugosi. *A probabilistic theory of pattern recognition*, volume 31 of *Applications of Mathematics (New York)*. Springer-Verlag, New York, 1996. ISBN 0-387-94618-7. doi: 10.1007/978-1-4612-0711-5. URL <https://doi.org/10.1007/978-1-4612-0711-5>.
- Harry Dym. *Linear algebra in action*, volume 78 of *Graduate Studies in Mathematics*. American Mathematical Society, Providence, RI, 2007. ISBN 978-0-8218-3813-6; 0-8218-3813-X.
- David Gilbarg and Neil S. Trudinger. *Elliptic partial differential equations of second order*, volume 224 of *Grundlehren der Mathematischen Wissenschaften [Fundamental Principles of Mathematical Sciences]*. Springer-Verlag, Berlin, second edition, 1983. ISBN 3-540-13025-X. doi: 10.1007/978-3-642-61798-0. URL <http://dx.doi.org/10.1007/978-3-642-61798-0>.

- Ian Goodfellow, Yoshua Bengio, and Aaron Courville. *Deep learning*. Adaptive Computation and Machine Learning. MIT Press, Cambridge, MA, 2016. ISBN 978-0-262-03561-3.
- Jack K. Hale. *Asymptotic behavior of dissipative systems*, volume 25 of *Mathematical Surveys and Monographs*. American Mathematical Society, Providence, RI, 1988. ISBN 0-8218-1527-X.
- Trevor Hastie, Robert Tibshirani, and Jerome Friedman. *The elements of statistical learning*. Springer Series in Statistics. Springer-Verlag, New York, 2001. ISBN 0-387-95284-5. doi: 10.1007/978-0-387-21606-5. URL <https://doi.org/10.1007/978-0-387-21606-5>. Data mining, inference, and prediction.
- Morris W. Hirsch and Stephen Smale. *Differential equations, dynamical systems, and linear algebra*. Academic Press [A subsidiary of Harcourt Brace Jovanovich, Publishers], New York-London, 1974. Pure and Applied Mathematics, Vol. 60.
- David Hoff. Stability and convergence of finite difference methods for systems of nonlinear reaction-diffusion equations. *SIAM J. Numer. Anal.*, 15(6):1161–1177, 1978. ISSN 0036-1429. doi: 10.1137/0715077. URL <https://doi.org/10.1137/0715077>.
- Arieh Iserles. *A first course in the numerical analysis of differential equations*. Cambridge Texts in Applied Mathematics. Cambridge University Press, Cambridge, second edition, 2009. ISBN 978-0-521-73490-5.
- Yann Lecun, Léon Bottou, Yoshua Bengio, and Patrick Haffner. Gradient-based learning applied to document recognition. In *Proceedings of the IEEE*, pages 2278–2324, 1998.
- Dominic Masters and Carlo Luschi. Revisiting small batch training for deep neural networks. *arXiv preprint arXiv:1804.07612*, 2018.
- Rafael Monteiro. Data repository for the paper “Binary classification as a phase separation process”. <https://dx.doi.org/10.5281/zenodo.4005131>, September 2021a.
- Rafael Monteiro. Source code for the paper “Binary classification as a phase separation process”. https://github.com/rafael-a-monteiro-math/Binary_classification_phase_separation, September 2021b.
- David Mumford. Issues in the mathematical modeling of cortical functioning and thought. In *The Legacy of Norbert Wiener: A Centennial Symposium (Cambridge, MA, 1994)*, volume 60 of *Proc. Sympos. Pure Math.*, pages 235–260. Amer. Math. Soc., Providence, RI, 1997. doi: 10.1090/pspum/060/1460286. URL <https://doi.org/10.1090/pspum/060/1460286>.
- Wei-Ming Ni. *The mathematics of diffusion*, volume 82 of *CBMS-NSF Regional Conference Series in Applied Mathematics*. Society for Industrial and Applied Mathematics (SIAM), Philadelphia, PA, 2011. ISBN 978-1-611971-96-5. doi: 10.1137/1.9781611971972. URL <https://doi.org/10.1137/1.9781611971972>.
- Jeffrey Rauch and Joel Smoller. Qualitative theory of the FitzHugh-Nagumo equations. *Advances in Math.*, 27(1):12–44, 1978. ISSN 0001-8708. doi: 10.1016/0001-8708(78)90075-0. URL [https://doi.org/10.1016/0001-8708\(78\)90075-0](https://doi.org/10.1016/0001-8708(78)90075-0).
- Shai Shalev-Shwartz and Shai Ben-David. *Understanding Machine Learning: From Theory to Algorithms*. Cambridge University Press, USA, 2014. ISBN 1107057132.
- John C. Strikwerda. *Finite difference schemes and partial differential equations*. The Wadsworth & Brooks/Cole Mathematics Series. Wadsworth & Brooks/Cole Advanced Books & Software, Pacific Grove, CA, 1989. ISBN 0-534-09984-X.